Spectroscopy of radicals, clusters, and transition states using slow electron velocity-map imaging of cryogenically cooled anions

Daniel M. Neumark

Department of Chemistry, University of California, Berkeley, CA 94720, USA and Chemical Sciences Division, Lawrence Berkeley National Laboratory, Berkeley, CA 94720, USA.

Abstract:

Slow electron velocity-map imaging of cryogenically cooled anions (cryo-SEVI) is a high resolution variant of anion photoelectron spectroscopy that has been applied with considerable success over the years to the study of radicals, size-selected clusters, and transition states for unimolecular and bimolecular reactions. Cryo-SEVI retains the versatility of conventional anion photoelectron spectroscopy while offering sub-meV resolution, thereby enabling the resolution of vibrational structure in the photoelectron spectra of complex anions. This article describes recent experiments in our laboratory using cryo-SEVI, including a new research direction in which anions are vibrationally pre-excited with an infrared laser pulse prior to photodetachment.

Introduction:

Anion photoelectron spectroscopy (PES) is a versatile experimental technique that enables detailed characterization of the neutral species created when an electron is photodetached from a negative ion.[1] In its canonical manifestation, mass-selected anions are photodetached at a fixed photon energy. The resulting photoelectron kinetic energy and angular distributions reveal information on the energetics, structure, and vibronic spectroscopy of the neutral. Anion PES has provided electron affinities for a wide range of atomic and molecular species.[2-3] Depending on the photon energy, PES can characterize the ground and electronically excited states of a neutral in a single experimental measurement, yielding term energies and, in favorable cases, vibrational structure in each of the accessible electronic states. Since photodetachment can access neutral electronic states of different spin multiplicity, PES provides a direct measure of singlet-triplet splittings and other spectroscopically challenging energetics.[4] In addition to these appealing capabilities, the neutral species that one can access by photodetachment are of considerable interest. PES is well suited to study open-shell radicals, which can be difficult to study experimentally due to their transient nature, through photodetachment of their closed-shell anions.[5-6] Since anion PES is inherently a mass-selective technique, it can also be applied to the anion clusters generated by laser-vaporization or electron impact sources and thus yield photoelectron spectra of size-selected clusters.[7-11] Finally, photodetachment of stable anions can access the transition states of unimolecular[12-13] and bimolecular chemical reactions,[14-15] in which case anion PES serves as a powerful spectroscopic probe of transition states.

The versatility of anion PES is, however, limited by its energy resolution, which is typically on the order of 10-30 meV, or 100-300 cm^{-1}. At this resolution, one can readily resolve electronic structure, but the observation of vibrational structure in clusters and polyatomic molecules can be more challenging, particularly in the presence of low-frequency vibrations and Franck-Condon (FC) activity in multiple vibrational modes. These considerations have led to efforts in our laboratory and elsewhere to improve the resolution of anion PES while retaining its versatility. [16]

Our first attempts at higher resolution experiments focused on anion zero electron kinetic energy (ZEKE) spectroscopy, inspired by the work by Muller-Dethlefs and Schlag on the photoionization of neutral molecules.[17-18] In their demonstration of this technique, NO was ionized *via* resonant two-color ionization, and electrons with nearly zero electron kinetic energy were detected as the photon energy was scanned. The underlying idea is that whenever the ionizing laser energy is just enough to access a cation state, one observes zero energy electrons. In this way, they were able to resolve individual rotationally resolved transitions between NO and NO$^+$, achieving an energy resolution on the order of 1 cm^{-1}. The mechanism of ZEKE electron production of neutrals is more complex than first believed and involves field ionization of high-lying Rydberg states rather than direct ionization.[19] Negative ions, on the other hand, do not have Rydberg states. Nonetheless, we initiated analogous experiments on negative ions starting in the late 1980's based on the selective detection of near-zero energy electrons produced by photodetachment with a tunable laser,[20] and were able to obtain ZEKE spectra with an

energy resolution of 1-2 cm^{-1} for a series of semiconductor clusters,[21] open-shell van der Waals clusters,[22] and, by photodetachment of IHI‾, the transition state of the I + HI reaction in which reactive resonances were spectroscopically resolved for the first time.[23] Anion ZEKE experiments with similar resolution were also carried out by Boesl on I‾(H$_2$O), FeO‾, and other anions. [24-25]

These experiments proved very challenging and were limited in generality by the Wigner threshold law,[26-27]

$$\sigma \propto (eKE)^{\ell+1/2} \qquad (1)$$

which dictates that at low electron kinetic energy (eKE), the photodetachment cross section σ scales with (eKE)$^{l+1/2}$, where l is the orbital angular momentum of the photoelectron. For anion ZEKE spectroscopy, where only electrons with near zero kinetic energies are detected, the near-threshold photodetachment cross section thus becomes vanishingly small with increasing angular momentum, so the technique works only for s-wave (l=0) detachment.

These constraints led to the development of slow-electron velocity-map imaging (SEVI) in our laboratory.[28] This technique was enabled by the many advances in ion and photoelectron imaging since the advent of ion imaging experiments in 1987,[29] particularly the development of velocity-map imaging (VMI) by Eppink and Parker[30], first applied to negative ions by Sanov.[31] In photoelectron VMI experiments, one typically images all of the photoelectrons onto a CCD camera and in principle can obtain the full photoelectron kinetic energy and angular distribution with a single measurement. In SEVI, we take advantage of the fact that the energy resolution of VMI is best for slow electrons, so our VMI electron optical setup is designed to preferentially detect electrons with low kinetic energies, yielding an energy resolution as high as 1-2 cm^{-1} for the slowest electrons for electrons with kinetic energy below 100 cm^{-1}. Further improvements result from trapping the anions in a radio frequency octupole trap held at 5 K and periodically filled with a low pressure He/H$_2$ gas mixture.[32] The trapped ions then undergo buffer gas collisions that cool them to internal temperatures as low as 10 K, resulting in nearly all the anions being in their vibrational ground state and low rotational states. This improved version of the experiment, cryo-SEVI, leads to near-complete suppression of vibrational hot bands and narrow rotational profiles, enabling one to obtain high resolution spectra even for complex molecular anions and clusters.[33-34]

Variants of anion SEVI and cryo-SEVI have been reported by several laboratories, including those of Gibson,[35-36] Wang,[37-38] Garand,[39-40] Ning,[3, 41] and Heaven;[42-43] the instruments used in those studies have also achieved sub-meV electron energy resolution. More specialized techniques such as photodetachment microscopy[44-45] yield even better resolution but are less universally applicable.

Cryo-SEVI experiments in our laboratory and elsewhere were reviewed in 2018.[46] This perspective focuses on results obtained since then, with particular focus on the cryo-SEVI spectra of NO$_3$‾,[47] the hydrated metal oxide clusters TiO$_3$H$_2$‾ and ZrO$_2$H$_2$‾,[48-49] and the transition state precursor anions H$_2$CC‾

and F⁻(NH₃).[13, 50] In addition, a new experimental direction is discussed in which anions are pre-excited with an infrared (IR) laser prior to photodetachment.[51-52] This IR cryo-SEVI experiment probes the effect of vibrational excitation on the anion photoelectron spectrum and provides a new means to measure the vibrational spectrum of a gas phase negative ion.

Experimental

The current configuration of the cryo-SEVI instrument[32, 46] is shown in Figure 1. Anions are generated using a pulsed molecular beam combined with either an electron impact ionizer or a Smalley-type laser ablation source. Recently, Wang and co-workers[38] have coupled an electrospray source to a cryo-SEVI instrument. In our experiment, the anions pass through a series of ion optics including a skimmer held at a repulsive voltage, a collimating radiofrequency (RF) hexapole, and a mass-selecting RF quadrupole, before entering a RF octupole ion trap held at 5 K. Ions spend ~40 ms in the trap, where they are cooled to roughly 10 K *via* collisions with helium buffer gas before being extracted from the trap into a Wiley-McLaren mass spectrometer.[53] After traveling along a perpendicular time-of-flight path, the ions of interest are photodetached inside a seven-plate VMI spectrometer by a pulsed laser beam from a dye laser. In IR cryo-SEVI experiments, the tunable infrared laser used to pre-excite the anions is spatially and temporally overlapped with the photodetachment pulse, as this configuration was found to give the highest IR-induced signals.

Photoelectrons are analyzed with a position-sensitive detector comprising two chevron-stacked microchannel plates coupled to a phosphor screen. A CCD camera takes a 768 × 768 pixel image of the phosphor screen each experimental cycle. The electron spots are event-counted, centroided, and binned into a 1024 × 1024 pixel grid. We have recently implemented new additions to the event-counting and centroiding algorithm that enable centroid analysis of overlapping electron spots, thereby improving the rate of data collection.[54] Photoelectron centroids are accumulated over several thousand experimental cycles into a single velocity-mapped image, and the radial and angular distributions of the images are calculated using the Maximum Entropy Velocity Legendre Reconstruction (MEVELER) method[55] or the more recently developed MELEXIR (Legendre Expanded Image Reconstruction) method.[56] The electron kinetic energy (eKE) distributions are related to the radial distributions by acquiring images of the well characterized photodetachment transitions of various atomic anions, such as O⁻, at several different photon energies.[57]

Since the VMI spectrometer has a roughly constant resolution Δv in velocity space and kinetic energy is proportional to v^2, the slowest photoelectrons are measured with the highest kinetic energy resolution ΔeKE. For this reason, cryo-SEVI spectra are acquired by first taking an overview spectrum at a relatively high detachment energy, comparable to conventional PES, and taking subsequent spectra at detachment energies slightly above the features of interest. Narrow high-resolution windows of these spectra are concatenated and appropriately scaled to create one high-resolution photoelectron

spectrum. Cryo-SEVI spectra are plotted as a function of electron binding energy (eBE), determined by eBE = hv − eKE, which is independent of the detachment photon energy.

Along with their kinetic energy distributions, VMI gives information about the angular distribution of the detached photoelectrons (PAD) for each transition. For single-photon detachment using linearly polarized light, the PAD is given by[58-59]

$$\frac{d\sigma}{d\Omega} = \frac{\sigma_{tot}}{4\pi}\left(1 + \beta P_2(\cos\theta)\right) \qquad (2)$$

where σ_{tot} is the total photodetachment cross-section, $P_2(x)$ is the second order Legendre polynomial, θ Is the angle of the photoelectron velocity vector relative to the laser polarization axis, and β is the anisotropy parameter, which ranges between -1 for perpendicular and +2 for parallel detachment. The variation of the anisotropy parameter as a function of eKE reflects the symmetry and angular momentum of the orbital from which the electron is detached.

Vibronic coupling in the NO$_3$ radical:

NO$_3$ was one of the first radicals to be spectroscopically observed,[60] and it plays a key role in atmospheric chemistry as an oxidizing agent in the nighttime troposphere.[61] Its spectroscopy is complex owing to the presence of two excited states, the $\tilde{A}^2E''$ and $\tilde{B}^2E'$ states, that lie 0.876 and 1.873 eV, respectively, above the ground $\tilde{X}^2A_2'$ state. While the $\tilde{B}^2E'$ - $\tilde{X}^2A_2'$ electronic transition has been studied by absorption, laser-induced fluorescence, and dispersed fluorescence,[62-66] the $\tilde{A}^2E''$ - $\tilde{X}^2A_2'$ transition is optically forbidden and is thus very weak.[67-68] Figure 2 shows an energy level diagram of electronic states of NO$_3$ and its vibrational modes.

In 1991, we reported the photoelectron spectrum of the nitrate anion, NO$_3^-$ in order to explore the vibrational and electronic spectroscopy of the NO$_3$ radical.[69] The anion photoelectron (PE) spectrum yielded several notable results. We saw photodetachment not only to the ground $\tilde{X}^2A_2'$ state of NO$_3$, but also to the previously unobserved $\tilde{A}^2E''$ state; while the $\tilde{A}$ state is optically dark with respect to the neutral $\tilde{X}$ state, it is accessible via one-electron photodetachment from the anion $\tilde{X}^1A_1$ state.

The ground state band obtained by photodetachment at 266 nm is shown in Figure 3a. From the vibrational origin, labeled 0_0^0, we obtained an electron affinity (EA) of 3.937 eV for the NO$_3$ radical. This band also reveals considerable vibrational structure. Peak b, lying 1057 cm^{-1} above the vibrational origin, was assigned to the 1_0^1 transition based on the ν_1 symmetric stretch frequency inferred from dispersed fluorescence from the NO$_3$ $\tilde{B}^2E'$ state. Most surprising, however, was the observation of a progression of peaks spaced by ~360 cm^{-1}, assigned to transitions involving the ν_4 in-plane bend as indicated in Figure 3a. In the D$_{3h}$ point group, this is a non-totally symmetric mode with e$'$ symmetry. Photodetachment transitions involving odd changes in the quantum number of this mode, such as the

4_0^1 transition, are Franck-Condon forbidden and thus should not appear in the photoelectron spectrum. We attributed these nominally forbidden peaks to pseudo-Jahn-Teller coupling with the NO_3 $\tilde{B}$ state, based on similar reasoning by Cederbaum and co-workers[70] used to explain the photoelectron spectrum of isoelectronic BF_3, an interpretation supported by subsequent theoretical work on NO_3.[71]

In 2007, Stanton[72] analyzed the spectroscopic data involving the ground state of NO_3 and proposed that the previously observed feature[73] at 1492 cm⁻¹ in its infrared spectrum was not the ν_3=1 fundamental of the degenerate antisymmetric stretch, but instead was the $\nu_1+\nu_4$ combination band. Subsequent work by Stanton[74-75] suggested that the ν_1 and ν_3 frequencies are both just above 1000 cm⁻¹, and that the feature assigned to the 1_0^1 transition in Figure 3a was predominantly the Franck-Condon forbidden 3_0^1 transition. A paper in 2018 by Hirota[76] questioned the existence of strong vibronic coupling between the $\tilde{X}$ and $\tilde{B}$ states, and proposed that peak a in the photoelectron spectrum was the Franck-Condon allowed 4_1^1 hot band transition rather than the F-C forbidden 4_0^1 transition.

This body of work motivated us to re-investigate the NO_3^- photoelectron spectrum using cryo-SEVI.[47] A representative set of spectra is shown in Figure 3b. The grey spectrum is an overview spectrum taken at hν=35137 cm⁻¹, while the black spectra represent three higher resolution composite spectra that have been concatenated and normalized to the overview spectrum. There are several key points of comparison between the cryo-SEVI in Fig. 3b and photoelectron spectra in Fig. 3a. First, the peaks in the cryo-SEVI spectra, particularly in the black spectra, are on average 10 cm⁻¹ wide, considerably narrower than the corresponding features in the PE spectrum. The position of the vibrational origin, peak A, yields a refined value of 3.9289(14) eV for the electron affinity of NO_3. Secondly, the 4_1^1 hot band in the photoelectron spectrum has disappeared in the cryo-SEVI spectrum, a consequence of better vibrational cooling in the latter spectrum. In contrast, peak a in the PE spectrum, assigned to the 4_0^1 transition, is clearly present in the cryo-SEVI spectrum as peak B and thus is not a hot band. Hence the alternative assignment proposed by Hirota is incorrect.

The third point to make is that the relative intensities of the peaks in the cryo-SEVI spectra differ markedly from those in the PE spectrum. Moreover, the relative intensities in the overview and high resolution cryo-SEVI spectra are very different. For example, the relative intensity of the vibrational origin, peak A, clearly drops relatively to that of peak B, the 4_0^1 transition, as we progress from the PE spectrum to the overview spectrum and then to the high-resolution composite spectrum. These spectra are taken at progressively lower photon energies, so the eKEs of the two peaks are dropping in this progression of spectra. According to the Wigner threshold law, Eq. (1), the photodetachment cross section drops with decreasing eKE, but it drops more abruptly at higher values of l. Hence, peak A appears to undergo photodetachment at a higher value of l than peak B.

These results can be explained through consideration of the selection rules for molecular photodetachment.[77-78] Photodetachment to the NO_3 ground state involves removal of an electron from an a_2' molecular orbital and can occur by p-wave but not s-wave detachment. Hence, near threshold, p-

wave detachment is the lowest allowed partial wave for the vibrational origin and all Franck-Condon allowed transitions. Peak B, the 4_0^1 transition, is allowed only through vibronic coupling to the higher lying $\tilde{B}\,^2E'$ state, and photodetachment to the $\tilde{B}\,^2E'$ state, in which an e' electron is removed, can occur via s-wave detachment. Since the vibronic wavefunction for the ν_4=1 level of the $\tilde{X}\,^2A_2'$ state is mixed with the ground vibrational level (or other totally symmetric vibrational levels) of the $\tilde{B}\,^2E'$ state, the 4_0^1 transition can occur via s-wave detachment. These considerations explain the experimental result that the intensity of peak A drops off more rapidly than that of peak B as the eKE is lowered, and lead to the somewhat counterintuitive result that at low eKE, the cryo-SEVI spectrum is dominated by vibronically allowed rather than FC allowed transitions.

One also notes that the intensity dependence of peak D on eKE is more similar to peak B than peak A. Peak D is thus also assigned to a vibronically allowed rather than FC allowed transition. This peak corresponds to an NO_3 vibrational frequency of 1044 cm^{-1}, which could be either the ν_1 fundamental or the ν_3 fundamental proposed by Stanton. The intensity dependence of this peak supports its assignment to the vibronically allowed 3_0^1 transition rather than the FC allowed 1_0^1 transition, in agreement with Stanton's value for the ν_3 frequency. Moreover, the eKE-dependent photoelectron angular distributions for peaks B and D are similar to one another and differ considerably from that of peak A.[47] Differing PADs across a photodetachment band are a well-known means of distinguishing FC allowed transitions from those allowed by vibronic coupling,[79-80] and in this case offer further support for the assignment of peaks B and D to the latter type of transition.

Water splitting by TiO$_2^-$ and ZrO$_2^-$

There is considerable interest in understanding the interaction of water with TiO_2 and ZrO_2.[81-82] For example, photocatalyzed water splitting on TiO_2 and ZrO_2 surfaces has the potential to play a key role in solar-powered fuel cells.[83-85] These considerations have motivated theoretical[86-89] and experimental[90-93] investigations of clusters of water with TiO_2 and ZrO_2. Electronic structure calculations by Dixon and co-workers on neutral $TiO_2 \cdot H_2O$ and $ZrO_2 \cdot H_2O$ clusters show that water splitting to form a dihydroxy species (*i.e.* $TiO(OH)_2$) is highly exothermic and proceeds over a small barrier.[86-87] By carrying out photoelectron spectroscopy of the anions $TiO_2^- \cdot H_2O$ and $ZrO_2^- \cdot H_2O$, one can determine whether dissociative chemisorption occurs in the anions and if it does, explore the spectroscopy of the neutral di-hydroxy species. Previous conventional anion photoelectron spectra did indeed suggest that $TiO_2^- \cdot H_2O$ is a di-hydroxide,[90] but no vibrational structure was resolved. We thus decided to investigate both $TiO_2^- \cdot H_2O$ and $ZrO_2^- \cdot H_2O$ with cryo-SEVI combined with electronic structure calculations.

The cryo-SEVI spectra of the bare anions TiO_2^- and ZrO_2^- are very simple, each showing short progressions in the totally symmetric stretch and bend modes.[94] The corresponding spectra of $TiO_2^- \cdot H_2O$ and $ZrO_2^- \cdot H_2O$ shown in Figures 4 and 5, respectively, are considerably more complex and differ substantially from one another.[48-49] The overview $TiO_2^- \cdot H_2O$ spectrum (in blue) has a pronounced

progression (A1, A3, A7, A11) with a characteristic peak spacing of 678 cm^{-1}, along with multiple smaller features. Higher resolution spectra (in black) reveal an additional series of peaks B1-B11 that are not evident in the overview spectrum. Moreover, the photoelectron angular distributions (PADs) for the A and B peaks are quite distinct; the anisotropy parameter β is around 1.5 for the A peaks and 0 for the B peaks. The $ZrO_2^-\cdot H_2O$ spectrum is much more congested, and there are several doublets (B/C, O/P, etc) where the peak spacing is only $\sim$5 cm^{-1}.

To interpret these results, Franck-Condon simulations based on electronic structure calculations were carried out. Results from $ZrO_2^-\cdot H_2O$ are shown in Figure 6 and are very similar to those found for $TiO_2^-\cdot H_2O$. For both species, the lowest energy anions and neutrals are the "chemisorbed" *cis*-dihyrodroxy $MO(OH)_2$ structures, with *trans* structures lying less than 10 meV higher. The barriers for *cis-→trans* conversion are calculated to be 0.100 and 0.091 eV for Ti and Zr, respectively. The "physisorbed" $MO_2^-\cdot H_2O$ structures are higher in energy by 2-3 eV. In light of these results, we will refer to these clusters from now on as $MO(OH)_2^{0/-}$. While the $TiO(OH)_2^{0/-}$ complexes are planar, the $ZrO(OH)_2^{0/-}$ complexes are not, with dihedral angles of 23.0° and 29.2°, respectively.[48] This non-planarity has a significant effect on the cryo-SEVI spectra as discussed below.

Franck-Condon simulations of the $TiO(OH)_2^-$ spectrum are shown as red sticks in Figure 4. The simulations assume all anions are in their vibrational ground state and have the *cis*-isomeric form. They match the structure in the overview spectrum, including the labelled A peaks, very well, and enable assignment of the A peaks to progressions in totally symmetric vibrational modes of $TiO(OH)_2$. Peak A1 is assigned to the vibrational origin (0_0^0), yielding an adiabatic electron affinity of 1.259(4) eV for $TiO(OH)_2$. The peaks spaced by 413 cm^{-1} (A1, A3, A7, A11) are assigned to the 3_0^n progression in the Ti-OH symmetric stretch. Additional peaks (A2, A6, A10) are assigned to the $4_0^1 3_0^n$ progression involving excitation of the ν_4 Ti-OH symmetric wag at 413 cm^{-1}, and several smaller peaks are assigned to excitation of other totally symmetric vibrations.

However, none of the B peaks appear in the FC simulations. This observation, along with the different PADs seen for the B peaks,[49] suggests that they involve FC-forbidden transitions of non-totally symmetric vibrational modes that become allowed only through Herzberg-Teller coupling with a low-lying excited state of neutral $TiO(OH)_2$. As seen in NO_3, effects of this type also lead to differences in the low-energy photodetachment cross sections for peaks that are vibronically vs. FC-allowed, and indeed the B peaks are seen only in the high-resolution scans where the eKE is low. The spacing between peaks A1 and B1 is 60 cm^{-1}, which is close to the calculated frequency for the ν_8 umbrella mode of $TiO(OH)_2$, a non-totally symmetric mode with b_1 symmetry, and in fact all the B peaks can be assigned to excitations of this mode. Hence, we attribute the B peaks to the presence of Herzberg-Teller coupling between the $^1A_1$ ground state and an as yet unidentified $^1B_1$ excited state of $TiO(OH)_2$.

FC analysis of the $ZrO(OH)_2^-$ spectrum revealed two major differences that explain why its appearance is so different from the $TiO(OH)_2^-$ spectrum. First, as mentioned above, the anion and neutral Zr

complexes are non-planar with different dihedral angles. Hence, a progression in the low frequency umbrella mode (ν_{12}) of the neutral is FC allowed, as opposed to being only vibronically allowed as was the case in the TiO(OH)$_2^-$ spectrum, leading to many more closely spaced peaks in the ZrO(OH)$_2^-$ spectrum. This effect alone, however, does not explain the closely spaced doublets in the ZrO(OH)$_2^-$ spectrum. These doublets and most other features can be explained by assuming equal population of both nearly degenerate *cis* and *trans* isomers of ZrO(OH)$_2^-$. Electronic structure calculations find the two isomers to have nearly identical electron affinities but slightly different vibrational frequencies in several low frequency, FC active modes. Hence, only one vibrational origin is observed, peak A at 1.1616(7) eV, but peaks B and C are split by 4 cm^{-1} because the vibrational frequency of the ν_{12} umbrella mode is 65 cm^{-1} for the *cis* isomer and 69 cm^{-1} for the *trans* isomers. The FC simulations for the two isomers are shown by the red (*cis*) and blue (*trans*) sticks in Figure 5. While the fit is not perfect, it does reproduce most of the experimental features and shows that there is more FC activity from the *trans* than from the *cis* isomer.

Taken together, the TiO(OH)$_2^-$ and ZrO(OH)$_2^-$ spectra show how subtle changes in structure can have major effects on the photoelectron spectrum. Each spectrum has its own complexities: TiO(OH)$_2^-$ from Herzberg-Teller coupling and ZrO(OH)$_2^-$ from the combination of two isomers being present as well as non-planar anion and neutral geometries.

The question arises as to why only one anion isomer contributes to the TiO(OH)$_2^-$ spectrum whereas two contribute to the ZrO(OH)$_2^-$ spectrum, given that the relative energetics of the two isomers are very similar in the Ti and Zr complexes as are the barriers to *cis-*→*trans* conversion. The differences between the two systems was attributed to differing conditions in the laser vaporization source used to generate the clusters. For example, the bond enthalpy of Zr-O exceeds that of Ti-O by nearly 100 kJ/mol, so the additional exothermicity associated with metal oxidation might lead to a different isomer population when the hot clusters are cryogenically cooled.

Transition state spectroscopy on H$_2$CC isomerization and the F+NH$_3$ reaction

Negative ion photodetachment has been shown to be a novel method of probing the transition states of benchmark unimolecular and bimolecular reactions.[14, 95-96] The underlying concept is that if a stable negative ion has a geometry similar to the neutral transition state for a chemical reaction, then photodetachment of the anion will access the transition state, and the resulting photoelectron spectrum can reveal resolved vibrational structure characteristic of the transition state region. Early examples include using the photoelectron spectroscopy of the vinylidene anion, H$_2$CC$^-$, to probe the dynamics of neutral vinylidene isomerization to acetylene (HCCH).[12, 97] There have also been numerous studies of several bimolecular hydrogen transfer reactions *via* photodetachment of the appropriate hydrogen bonded negative ion, such as photodetaching FH$_2^-$ to investigate the transition state of the F + H$_2$ reaction.[98] The higher resolution offered initially by anion ZEKE spectroscopy and, more recently, cryo-SEVI, have revealed additional vibrational features not seen in conventional photoelectron spectra, most

notably the spectroscopic observation of reactive resonances in the I + HI and F + H_2 reactions *via* photodetachment of IHI^- and FH_2^-.[23, 99] Entrance channels for the Cl + H_2 and F + CH_4 reactions have also been probed.[100-101] Here, recent results are described in which cryo-SEVI spectra of H_2CC^- and FNH_3^- are used to probe the transition states for the unimolecular $H_2CC \rightarrow HCCH$ isomerization reaction[13] and the bimolecular reaction F + $NH_3 \rightarrow HF + NH_2$.[50]

Vinylidene, H_2CC, is the simplest carbene and as such is of considerable interest in organic chemistry.[102] As shown schematically in Figure 7a, it lies 1.925 eV above acetylene and can isomerize to HCCH over a small (0.13 eV) barrier.[103-105] The isomerization reaction is the simplest 1,2-hydrogen shift and is thus a benchmark chemical reaction.[106] This consideration has motivated many experimental[12, 107-109] and theoretical[110-114] studies of how the vibrational energy levels of H_2CC and HCCH are coupled to one another. One approach to this problem has been to map out the excited vibrational energy levels of HCCH that lie above the H_2CC minimum and search for perturbations with H_2CC levels.[108, 115-116] A more direct approach, developed by Lineberger,[12] makes use of the fact that that H_2CC^- is the stable anionic form of H_2CC, and that photodetachment of this species directly accesses the neutral H_2CC well, corresponding to the $\tilde{X}\ ^1A_1$ state of vinylidene. The resulting photoelectron spectrum shows resolved vibrational structure. Remarkably, the peaks in the singlet band are notably broader than those seen upon photodetachment to the higher-lying $\tilde{a}\ ^3B_2$ triplet state of H_2CC that is known to have a much larger barrier to isomerization.[117] On this basis, the broadening of the peaks in the singlet spectrum was attributed to isomerization to acetylene on a sub-picosecond time scale. This result motivated multiple investigations of H_2CC^- in our laboratory and in Canberra to map out photodetachment to both single and triplet states of H_2CC with high resolution and to explore vibrational autodetachment in H_2CC^-.[13, 117-118] Below, results are described in which cryo-SEVI combined with quantum dynamics calculations probes how (or if) H_2CC vibrations mix with high-lying HCCH vibrational states.

Figure 7b shows cryo-SEVI spectra of H_2CC^- and D_2CC^- along with their peak assignments; blue, black, and red traces are overview spectra, high-resolution composite spectra, and FC simulations, respectively.[13] The high-resolution D_2CC^- spectra show no evidence of spectral broadening beyond that consistent with an unresolved rotational profile, and this is also the case for most features in the H_2CC^- spectrum. However, the situation is more complex upon excitation of the ν_5 antisymmetric stretch or ν_6 rocking vibration of H_2CC, both of which are non-totally symmetric. The weak 6_0^1 and 6_0^2 peaks in the H_2CC^- spectrum are notably broader than the corresponding peaks in the D_2CC^- spectrum. The 5_0^1 transition, which is a single peak in the D_2CC^- spectrum, looks to be a multiplet of closely spaced peaks in the H_2CC^- spectrum. Hence, excitation of the ν_5 and ν_6 vibrations appears to yield much stronger coupling to the HCCH well than excitation of the totally symmetric vibrations ν_2 and ν_3 vibrations. This interpretation is supported by quantum dynamics calculations, displayed in Figure 8, that show that the wavefunctions of the 6^2 and 5^1 H_2CC vibrational levels have substantial amplitude at the HCCH geometry (upper right corner). The overall interpretation of these results is that there is

coupling between H_2CC and HCCH vibrational energy levels, but this coupling is vibrationally state-specific and only activated upon excitation of the ν_5 and ν_6 modes of H_2CC.

As mentioned above, negative ion photodetachment is uniquely suited to carry out transition state spectroscopy experiments on bimolecular reactions. Much of this work has been carried out on triatomic systems. However, a cryo-SEVI experiment on CH_3OHF^- successfully mapped out a series of exit channel Feshbach resonances corresponding to metastable vibrational states of the $CH_3O\cdot HF$ complex that predissociate to $CH_3O + HF$,[119] yielding considerably higher resolution than a previous study of this system via conventional photoelectron spectroscopy.[120]

We recently measured cryo-SEVI spectra of the related system FNH_3^- to investigate the bimolecular F + NH_3 reaction.[50] This reaction has been studied previously by infrared chemiluminescence[121-123] and with crossed molecular beams scattering.[124] Potential energy surfaces for this reaction have been reported[125-126] and dynamics on these surfaces were explored using quasi-classical trajectory calculations.[126-127]

The relevant energetics and geometries for this system are shown in Figure 9.[50] The reaction is exothermic by 1.3 eV and has a submerged barrier between reactant $F\cdot NH_3$ and product $FH\cdot NH_2$ complexes. The anion is strongly hydrogen-bonded with a calculated dissociation energy of 0.70 eV and has good geometric overlap with the neutral transition state. The goal of the experiment, then, was to observe vibrational structure associated with not only the product complex, as was seen in CH_3OHF^-, but also the transition state and reactive complex, and, possibly, dynamical resonances lying above the F + NH_3 reactant asymptote.

The experimental spectra are shown as blue (overview) and black (high resolution composite) traces in Figure 10; the lower two traces are simulated spectra from reduced dimensionality quantum dynamics calculations. The energies of the transition state and reactant asymptote are shown as grey and black arrows, respectively. There is substantial vibrational structure in the spectrum whose appearance evolves notably with increasing electron binding energy. Peaks a-j are spaced by about 300 cm^{-1}. They lie below the transition state energy and are attributed to resonances associated with the product complex that can undergo vibrational predissociation to $NH_2 + HF$. Quantum dynamics calculations of the resonance wavefunctions[50] show that the peaks correspond to progressions in the $NH_2\cdot HF$ hindered translational mode at 251 cm^{-1} and a more complex vibration at 829 cm^{-1} in which pseudo-rotation of the HF is coupled to NH_2 out-of-plane wagging. The out-of-plane motion is activated by the flattening of the NH_3 pyrimidal structure in the anion upon photodetachment to the $NH_2\cdot HF$ product complex.

At higher binding energy, peaks k-o are considerably broader. They lie in the energy range just above the transition state barrier in Figure 9, hence the neutral states have amplitude on both sides of the barrier. The vibrational structure responsible for these peaks is quite complex; quantum dynamics calculations show that the neutral states have three quanta of excitation in the HF stretch, along with excitations in the out-of-plane wagging mode of the NH_2 (~318 cm^{-1}) and a pseudo-rotation of the HF

11

moiety (655 cm^{-1}). Finally, peaks q-t lie above the reactant asymptote and thus represent reactive resonances that can in principle be accessed in F+NH$_3$ reactive scattering.

Overall, the F⁻NH$_3$ cryo-SEVI spectrum comprises a very rich resonance structure spanning the exit channel, the transition state region, and states above the reactant asymptote. In contrast to other bimolecular transition states studied with this technique,[119] the vibrational structure cannot be explained in terms of a high-frequency hydrogen atom motion and a much lower frequency stretching motion involving the heavier atoms. The complexity of the spectrum reflects the fact that F + NH$_3$ is not a simple hydrogen transfer reaction because the geometry of the NH$_3$ moiety evolves significantly en route to the HF + NH$_2$ products. Hence, assignment of the vibrational structure is possible only by comparison with multidimensional quantum dynamics calculations.

Vibrational pre-excitation of anions: IR cryo-SEVI

A primary goal of cryo-SEVI is to use cryogenic cooling to bring the anions into their ground vibrational state, thereby eliminating vibrational hot bands in the photoelectron spectrum, and to rotationally cool the anions as much as possible to obtain narrow rotational profiles. However, the extent to which one can extract vibrational frequencies from these spectra and, more generally, learn about the neutral potential energy surface accessed by photodetachment is limited by the selection rules that govern photoelectron spectroscopy.

The intensities of vibrational transitions in photoelectron spectra are typically governed by Franck-Condon factors. In the absence of vibronic coupling, this means that starting from the anion ground vibrational state, one only observes progressions in totally symmetric vibrational modes for which there is a normal coordinate displacement upon photodetachment. For symmetry reasons, there is no such displacement for non-totally symmetric modes, and while CH, NH, and OH stretches in molecules can be totally symmetric, changes in the corresponding bond lengths upon anion photodetachment are generally very small.[128-130] Hence, the situation on the left side of Figure 11 holds, in which transition intensities from the anion ground state to the $v = 1$ level of a non-totally symmetric mode or a mode in which there is no normal coordinate displacement are either zero by symmetry or negligibly small. However, excitation of the $v = 1$ level of one of these modes in the anion results in a fully FC-allowed transition to the neutral $v = 1$ level, as shown on the right side of Figure 11, leading to new features in the photoelectron spectrum.   Hence, IR pre-excitation of negative ions has the potential to access previously unseen neutral vibrational states and, more generally, expand the range of nuclear configurations probed on the neutral potential energy surface.

In order to carry out experiments of this type, we have incorporated a tunable IR laser into our experiment that excites the cryogenically cooled anions prior to photodetachment. This new experimental configuration, IR cryo-SEVI, has been carried out on a diatomic anion, OH⁻,[51] and, more recently, on the polyatomic vinoxide anion CH$_2$CHO⁻.[52] The OH⁻ anion served as a first demonstration of the technique; it is a special case in the sense that the cryo-SEVI spectrum is fully rotationally resolved[51]

and the gas phase infrared spectrum is well characterized.[131-132] The vinoxide results illustrate the potential and complexity of IR cryo-SEVI, most notably the observation of effects associated with anharmonic coupling between vibrational modes in the anion and neutral as well as the dependence of these effects on the vibrational frequency of the pre-excited mode.

The hydroxide anion OH⁻ has been extensively studied by photodetachment, including rotationally resolved threshold photodetachment measurements by Lineberger[133] and Wester[134] as well as photodetachment microscopy experiments by Blondel.[130] The rotationally-resolved infrared spectrum of OH⁻ was measured by Saykally using velocity-modulated IR spectroscopy,[131, 135] while the open-shell X $^2\Pi$ ground state of the OH radical has been characterized extensively using microwave spectroscopy[136-137] and other methods.[138-139] This body of work leads to the energy level diagram in Figure 12, showing the rovibrational structure of the $X\,^1\Sigma^+$ anion ground state and the two spin-orbit manifolds of OH.

Figure 13 shows the cryo-SEVI spectrum of OH⁻ without (black) and with (red) IR pre-excitation.[51] Both spectra are fully rotationally resolved and assigned; selected transitions are indicated in Figures 12 and 13. The two most intense IR-off transitions, the R3(0) and R1(0) transitions, originate from the (v=0,J=0) state of the anion. The relative intensities of these peaks compared to those originating from higher lying anion rotational states yields a rotational temperature of ~20 K. The red trace shows the IR cryo-SEVI spectrum where the IR laser is tuned to the R(0) transition of the anion at 3591 cm^{-1}, exciting anions from the (0,0) level to (1,1) level. One observes significant depletion of the R3(0) and R1(0) transitions, while five new transitions originating from the (1,1) anion appear that are assigned in Figure 13. These are "sequence band" transitions between the v=1 anion and neutral levels and are interspersed with the transitions originating from the anion v=0 level. One can also obtain a "vibrational action spectrum" by scanning the IR laser and following the change in intensity of one of the red IR-on features, as was done for the R3(1) peak at 14799 cm^{-1}.[51]

While the idea of IR cryo-SEVI seems simple in principle, the spectra in Figure 13 illustrate that at least for OH⁻, very cold ions and high photoelectron kinetic energy resolution are required. The red peaks resulting from vibrationally excited anions all lie within a few cm^{-1} of the nearest ground state feature and would thus be obscured if the resolution were sub-optimal or if the anions were warmer; the latter scenario would lead to more rotational features in the IR-off spectrum that overlap spectrally with the IR-on peaks. In addition, the fraction of vibrationally excited molecules would be reduced when higher rotational levels of the vibrational ground state are populated, as those require slightly different IR excitation frequencies.

The extension of IR cryo-SEVI to polyatomic molecules presents several challenges. First, although many infrared spectra of negative ions have been obtained through "tagging" experiments,[140-141] it is still the case that relatively few vibrational frequencies are known for gas phase anions. Secondly, at the few-cm^{-1} resolution of the cryo-SEVI instrument, one does not expect to resolve individual rotational transitions in polyatomic anions. Finally, the vibrational state excited by the IR laser may be

anharmonically coupled to nearby vibrational levels,[142] leading to more complexity in the resulting photoelectron spectrum than implied by the simple picture in Figure 11.

The vinoxide anion was selected as a suitable polyatomic since both the anion and neutral are reasonably well characterized. Photodetachment of the anion has been investigated in several experiments, [143-146] including a SEVI study in our group prior to the installation of cryogenic cooling.[147] The microwave,[148] infrared[149-150] and electronic spectra[151-155] of the vinoxy radical and its photodissociation dynamics[156] have also been reported. The electron affinity of vinoxy is 1.825 eV, which is convenient for photodetachment with a dye laser, and the SEVI spectrum exhibits some vibrational structure but is relatively sparse. Quantum chemistry calculations on the vinoxide anion at the B2PLYP-D3/aug-cc-pVTZ level of theory including anharmonicity find two strong infrared transitions, the ν_4 CO stretch at 1560 cm^{-1} and the ν_3 carbonyl CH stretch at 2512 cm^{-1}.[52] These two modes were thus targeted for our IR cryo-SEVI experiment, with the calculated frequencies taken as starting points for our search.

Figures 14a and b show photoelectron images of vinoxide with the IR laser off (a) and tuned to the ν_4 transition at 1570 cm^{-1} (b). The corresponding photoelectron spectra are shown in black and red, respectively, in Figure 14c. The vibrational origin (0_0^0) is the largest peak in the IR-off spectrum, and there is FC activity in the totally symmetric ν_9 (CCO bend), ν_7 (CC stretch), and ν_4 (CO stretch) modes. The additional rings in Figure 14b, indicated with arrows, represent hot-band transitions from the vibrationally excited anion and appear as small peaks below the vibrational origin in the red trace in Figure 14c. Figure 14d shows the (IR on)-(IR off) difference spectrum; here, the negative peaks represent ground state features that are depleted by the IR laser pulse, while the positive peaks are transitions from vibrationally excited anions. Peak assignments for the positive features are shown; the peak at lowest eBE is the 4_1^0 transition, and the other peaks are transitions from the ν_4=1 level of the anion to various vibrational states of vinoxy. The low eBE region of the IR-on photoelectron spectrum, showing a progression in the ν_9 mode ($4_1^0 9_0^n$), is very similar to the IR-off spectrum, except that the peaks in the IR-on spectrum are shifted to lower eBE by the anion ν_4 frequency. At larger eBE, however, the IR-on photoelectron spectrum is markedly different, showing FC activity in the ν_5 and ν_8 modes, which are not observed in the IR-off spectrum. A harmonic Franck-Condon simulation (Figure 14e) assuming all anions are in the ν_4=1 level simulates the IR-on spectrum very well. This agreement shows vibrational excitation of the anion ν_4 mode remains "in place" on the timescale of our experiment (~10 ns) and is well described within the harmonic approximation typically used for the interpretation of photoelectron spectra.

Results from excitation of the ν_3 mode at 2546 cm^{-1} are shown in Fig. 15. The top panel shows IR-off (black) and IR-on spectra (red), the middle panel is the difference spectrum, and the bottom panel shows a harmonic FC simulation starting from the anion ν_3=1 level. Clearly, the difference spectrum is much more complex than the ground state spectrum. Moreover, it is in poor agreement with the FC

simulation, which predicts a few ν_3 sequence band transitions (3^1_1, *etc.*) above the vibrational origin and no transitions below the origin. The experimental difference spectrum, in contrast, shows many small features below the origin, and a comparison to the FC simulation suggests that each ν_3 sequence band appears to be split into four closely spaced transitions.

These effects can be explained within the context of anharmonic coupling within the anion and neutral. Essentially, the nominal $\nu_3=1$ anion and neutral levels are mixed with nearby vibrational states, so that the individual vibrational eigenstates are linear combinations of multiple harmonic zero-order vibrational states. A near-quantitative agreement with experiment is obtained using a newly developed implementation of vibrational perturbation theory (VPT)[52, 157-161] that identifies relevant anharmonic couplings among nearly degenerate vibrational states and provides the contributions of the individual harmonic states to the vibrational eigenstate. The underlying concept is illustrated in Figure 16. In the absence of anharmonic coupling, photodetachment from the anion $\nu_3=1$ state $\left| \phi''_{\nu_3} \right\rangle$ accesses the corresponding neutral $\nu_3=1$ state $\left| \phi'_{\nu_3} \right\rangle$, leading to the 3^1_1 transition seen in the FC simulation. However, anharmonic coupling in the anion can mix the zero-order $\left| \phi''_{\nu_3} \right\rangle$ and $\left| \phi''_{\nu_4+\nu_8} \right\rangle$ states, resulting in a coupled anion eigenstate $\left| \chi''_i \right\rangle$ that can undergo photodetachment to the neutral $\left| \phi'_{\nu_4+\nu_8} \right\rangle$ state in addition to the $\left| \phi'_{\nu_3} \right\rangle$ state. Similarly, owing to anharmonic couplings in the radical, the neutral vibrational eigenstates $\left| \chi'_f \right\rangle$ are linear superpositions of the $\left| \phi'_{\nu_3} \right\rangle$ zero-order state and other nearby vibrational states, giving each of those neutral eigenstates ν_3 character.

Under these circumstances, the relative intensity of a transition between anion and neutral eigenstates $\left| \chi''_i \right\rangle$ and $\left| \chi'_f \right\rangle$ is given by

$$\left| \left\langle \chi_f' \middle| \chi_i'' \right\rangle \right|^2 = \left| \sum_{j,k} c_k' c_j'' \left\langle \phi_k' \middle| \phi_j'' \right\rangle \right|^2 \qquad (3)$$

The VPT analysis shows that the structure below the vibrational origin results primarily from anharmonic coupling within the anion, whereas above the origin the quartets corresponding to the ν_3 sequence band mostly reflect neutral anharmonic couplings. In fact, three of the peaks within these quartets can be considered to be polyads based on the $\nu_3=1$ neutral level, while the fourth peak results from photodetachment to neutral states involving $\nu_4 + \nu_8$ excitation.

The vinoxide study leads to several interesting conclusions. It demonstrates that IR cryo-SEVI can be applied to polyatomic anions.   Excitation of the vinoxide CO stretch at 1570 cm^{-1} yields a photoelectron spectrum that is readily interpreted and assigned within the harmonic approximation that is typically used for the interpretation of photoelectron spectra. The significant differences between the results at

1570 and 2546 cm^{-1} shows that at the higher vibrational frequency, effects attributed to anharmonic coupling in both the vinoxide anion and vinoxy radical are quite prominent but nonetheless can be analyzed using vibrational perturbation theory. The ability to spectroscopically determine which modes are coupled through anharmonic interactions complements previous work on intramolecular vibrational energy redistribution in polyatomic neutral molecules,[162-163] most notably the IR chemiluminescence studies of McDonald and co-workers.[142, 164] As further applications of IR cryo-SEVI are explored, the extent to which anharmonic coupling grows in with increasing vibrational excitation and complexity of the molecule will play a major role in understanding this new experimental method.

Concluding remarks:

Cryo-SEVI continues to be a powerful experimental tool that enables one to obtain high resolution photoelectron spectra for an array of negative ions ranging from transition metal and lanthanide atoms to complex, polyatomic clusters. While this article primarily focuses on experiments carried out in Berkeley, cryo-SEVI instruments are operating at several other laboratories in the US and elsewhere. From a personal perspective, there are two key questions regarding the future directions of the technique. First, what are the limits on the size and complexity of a target system for which cryo-SEVI will yield a well-resolved spectrum? The answer clearly depends on the extent of multi-mode Franck-Condon activity, or, put another way, how significant the geometry changes of the anion are upon photodetachment. It also depends on how effectively the anions can be cooled, as there is evidence that vibrational cooling in our cryogenic ion trap is incomplete for, say, polyatomic metal oxide cluster anions. Secondly, the IR cryo-SEVI experiment described herein has considerable potential. A primary goal of this work is its application to both unimolecular and bimolecular transition state spectroscopy systems, since vibrational excitation of the anion enlarges the Franck-Condon accessible transition state region and thus, in principle, enables a more complete mapping of the neutral potential energy surface on which the chemical reaction occurs. On the other hand, as the number of atoms and/or the infrared excitation energy increases, the interpretation of the resulting spectra becomes more complicated and, at the same time, more interesting, owing to the anharmonic coupling effects seen here for the vinoxide example. We thus hope in the near future to better understand the extent to which this new experiment can be applied to the many anions that have been studied by photoelectron spectroscopy and its variants.

Acknowledgments:

[1]   Lineberger, W. C., Once upon Anion: A Tale of Photodetachment. In *Annual Review of Physical Chemistry, Vol 64*, Johnson, M. A.; Martinez, T. J., Eds. 2013; Vol. 64, pp 21-36.

[2]   Rienstra-Kiracofe, J. C.; Tschumper, G. S.; Schaefer, H. F.; Nandi, S.; Ellison, G. B., Atomic and molecular electron affinities: Photoelectron experiments and theoretical computations. *Chem. Rev.* **2002,** *102*, 231-282.

[3]   Ning, C.; Lu, Y., Electron Affinities of Atoms and Structures of Atomic Negative Ions. *J. Phys. Chem. Ref. Data* **2022,** *51*, 021502.

[4]   Leopold, D. G.; Murray, K. K.; Miller, A. E. S.; Lineberger, W. C., METHYLENE - A STUDY OF THE X $^3B_1$ AND A $^1A_1$ STATES BY PHOTOELECTRON-SPECTROSCOPY OF CH_2^- AND CD_2^-. *J. Chem. Phys.* **1985,** *83*, 4849-4865.

[5]   Engelking, P. C.; Ellison, G. B.; Lineberger, W. C., Laser photodetachment electron spectrometry of methoxide, deuteromethoxide and thiomethoxide: electron affinities and vibrational structure of CH_3O, CD_3O, and CH_3S. *J. Chem. Phys.* **1978,** *69*, 1826-32.

[6]   Ervin, K. M.; Gronert, S.; Barlow, S. E.; Gilles, M. K.; Harrison, A. G.; Bierbaum, V. M.; Depuy, C. H.; Lineberger, W. C.; Ellison, G. B., Bond Strengths Of Ethylene and Acetylene. *J. Am. Chem. Soc.* **1990,** *112*, 5750-5759.

[7]   Leopold, D. G.; Ho, J.; Lineberger, W. C., Photoelectron-Spectroscopy of Mass-Selected Metal Cluster Anions .1. Cu_n^-, n= 1-10. *J. Chem. Phys.* **1987,** *86*, 1715-1726.

[8]   Posey, L. A.; Deluca, M. J.; Johnson, M. A., Demonstration of a pulsed photoelectron spectrometer on mass-selected negative ions: O^-, O_2^-, and O_4^-. *Chem. Phys. Lett.* **1986,** *131*, 170-4.

[9]   Cheshnovsky, O.; Taylor, K. J.; Conceicao, J.; Smalley, R. E., Ultraviolet photoelectron spectra of mass-selected copper clusters: Evolution of the 3d band. *Phys. Rev. Lett.* **1990,** *64*, 1785-1788.

[10]   Castleman, A. W., Jr.; Bowen, K. H., Jr., Clusters: Structure, Energetics, and Dynamics of Intermediate States of Matter. *J. Phys. Chem.* **1996,** *100*, 12911-12944.

[11]   Wu, H. B.; Desai, S. R.; Wang, L. S., Evolution Of the Electronic Structure Of Small Vanadium Clusters From Molecular to Bulklike. *Phys. Rev. Lett.* **1996,** *77*, 2436-2439.

[12]   Ervin, K. M.; Ho, J.; Lineberger, W. C., A Study Of the Singlet and Triplet States Of Vinylidene By Photoelectron Spectroscopy Of $H_2C=C^-$, $D_2C=C^-$, and $HDC=C^-$ - Vinylidene Acetylene Isomerization. *J. Chem. Phys.* **1989,** *91*, 5974-5992.

[13]   DeVine, J. A.; Weichman, M. L.; Laws, B.; Chang, J.; Babin, M. C.; Balerdi, G.; Xie, C. J.; Malbon, C. L.; Lineberger, W. C.; Yarkony, D. R.; Field, R. W.; Gibson, S. T.; Ma, J. Y.; Guo, H.; Neumark, D. M., Encoding of vinylidene isomerization in its anion photoelectron spectrum. *Science* **2017,** *358*, 336-339.

[14]   Neumark, D. M., Probing the transition state with negative ion photodetachment: experiment and theory. *Phys. Chem. Chem. Phys.* **2005,** *7*, 433-442.

[15]   Continetti, R. E.; Guo, H., Dynamics of transient species via anion photodetachment. *Chem. Soc. Rev.* **2017,** *46*, 7650-7667.

[16]   Neumark, D. M., Slow Electron Velocity-Map Imaging of Negative Ions: Applications to Spectroscopy and Dynamics. *J. Phys. Chem. A* **2008,** *112*, 13287-13301.

[17]   Muller-Dethlefs, K.; Sander, M.; Schlag, E. W., 2-Color Photoionization Resonance Spectroscopy of NO - Complete Separation of Rotational Levels of NO^+ at the Ionization Threshold. *Chem. Phys. Lett.* **1984,** *112*, 291-294.

[18]   Muller-Dethlefs, K.; Schlag, E. W., High-Resolution Zero Kinetic Energy (Zeke) Photoelectron Spectroscopy of Molecular Systems. *Annu. Rev. Phys. Chem.* **1991,** *42*, 109-136.

[19]   Reiser, G.; Habenicht, W.; Mullerdethlefs, K., THE IONIZATION-ENERGY OF NITRIC-OXIDE. *Chem. Phys. Lett.* **1988,** *152*, 119-123.

[20]   Kitsopoulos, T. N.; Waller, I. M.; Loeser, J. G.; Neumark, D. M., High Resolution Threshold Photodetachment Spectroscopy Of Negative Ions. *Chem. Phys. Lett.* **1989,** *159*, 300-306.

[21]   Arnold, C. C.; Neumark, D. M., Study Of Si_4 and Si_4^- Using Threshold Photodetachment (Zeke) Spectroscopy. *J. Chem. Phys.* **1993,** *99*, 3353-3362.

[22]   Zhao, Y. X.; Yourshaw, I.; Reiser, G.; Arnold, C. C.; Neumark, D. M., Study Of the $ArBr^-$, ArI^-, and KrI^- Anions and the Corresponding Neutral Van Der Waals Complexes By Anion Zero Electron Kinetic Energy Spectroscopy. *J. Chem. Phys.* **1994,** *101*, 6538-6551.

[23]   Waller, I. M.; Kitsopoulos, T. N.; Neumark, D. M., Threshold Photodetachment Spectroscopy Of the I+HI Transition-State Region. *J. Phys. Chem.* **1990,** *94*, 2240-2242.

[24]   Bassmann, C.; Boesl, U.; Yang, D.; Drechsler, G.; Schlag, E. W., Mass selective anion-ZEKE spectroscopy of the iodine-water cluster. *Int. J. Mass Spec. Ion Proc.* **1996,** *159*, 153-167.

[25]   Drechsler, G.; Boesl, U.; Bäsmann, C.; Schlag, E. W., Mass selected anion-zero kinetic energy photoelectron spectroscopy (anion-ZEKE): Ground and low excited states of FeO. *J. Chem. Phys.* **1997,** *107*, 2284-2291.

[26]   Wigner, E. P., On the behavior of cross sections near thresholds. *Phys. Rev.* **1948,** *71*, 1002-1009.

[27]   Rau, A. R. P., Threshold Laws. *Comments on Atomic and Molecular Physics* **1884,** *14*, 285-306.

[28]   Osterwalder, A.; Nee, M. J.; Zhou, J.; Neumark, D. M., High resolution photodetachment spectroscopy of negative ions via slow photoelectron imaging. *J. Chem. Phys.* **2004,** *121*, 6317-6322.

[29]   Chandler, D. W.; Houston, P. L., Two-dimensional imaging of state-selected photodissociation products detected by multiphoton ionization. *J. Chem. Phys.* **1987,** *87*, 1445-7.

[30]   Eppink, A. T. J. B.; Parker, D. H., Velocity map imaging of ions and electrons using electrostatic lenses: Applications in photoelectron and photofragment ion imaging of molecular oxygen. *Rev. Sci. Instrum.* **1997,** *68*, 3477.

[31]   Surber, E.; Sanov, A., Photoelectron imaging spectroscopy of molecular and cluster anions: CS_2^- and $OCS^-(H_2O)_{1,2}$. *J. Chem. Phys.* **2002,** *116*, 5921.

[32]   Hock, C.; Kim, J. B.; Weichman, M. L.; Yacovitch, T. I.; Neumark, D. M., Slow photoelectron velocity-map imaging spectroscopy of cold negative ions. *J. Chem. Phys.* **2012,** *137*, 224201.

[33]   Weichman, M. L.; DeVine, J. A.; Levine, D. S.; Kim, J. B.; Neumark, D. M., Isomer-specific vibronic structure of the 9-, 1-, and 2-anthracenyl radicals via slow photoelectron velocity-map imaging. *PNAS* **2016,** *113*, 1698-1705.

[34]   Kim, J. B.; Weichman, M. L.; Neumark, D. M., Structural Isomers of Ti_2O_4 and Zr_2O_4 Anions Identified by Slow Photoelectron Velocity-Map Imaging Spectroscopy. *J. Am. Chem. Soc.* **2014,** *136*, 7159-7168.

[35]   Cavanagh, S. J.; Gibson, S. T.; Gale, M. N.; Dedman, C. J.; Roberts, E. H.; Lewis, B. R., High-resolution velocity-map-imaging photoelectron spectroscopy of the O^- photodetachment fine-structure transitions. *Phys. Rev. A* **2007,** *76*, 052708.

[36]   Laws, B. A.; Levey, Z. D.; Sanov, A.; Stanton, J. F.; Schmidt, T. W.; Gibson, S. T., Velocity map imaging spectroscopy of C_2H^- and C_2D^-: A benchmark study of vibronic coupling interactions. *J. Chem. Phys.* **2022,** *157*, 044305.

[37]   León, I.; Yang, Z.; Liu, H.-T.; Wang, L.-S., The design and construction of a high-resolution velocity-map imaging apparatus for photoelectron spectroscopy studies of size-selected clusters. *Rev. Sci. Instrum.* **2014,** *85*, -.

[38]   Zhang, Y.-R.; Yuan, D.-F.; Wang, L.-S., Probing the electronic structure and spectroscopy of pyrrolyl and imidazolyl radicals using high-resolution photoelectron imaging of cryogenically cooled anions. *Phys. Chem. Chem. Phys.* **2022,** *24*, 6505-6514.

[39]   Kregel, S. J.; Thurston, G. K.; Zhou, J.; Garand, E., A multi-plate velocity-map imaging design for high-resolution photoelectron spectroscopy. *J. Chem. Phys.* **2017,** *147*, 094201.

[40]   Sagan, C. R.; Garand, E., Anion Resonances and Photoelectron Spectroscopy of the Tetracenyl Anion. *J. Phys. Chem. A* **2021,** *125*, 7014-7022.

[41]   Luo, Z.; Chen, X.; Li, J.; Ning, C., Precision measurement of the electron affinity of niobium. *Phys. Rev. A* **2016,** *93*, 020501.

[42]   Mascaritolo, K. J.; Dermer, A. R.; Green, M. L.; Gardner, A. M.; Heaven, M. C., Photodetachment spectroscopy of the beryllium oxide anion, BeO^-. *J. Chem. Phys.* **2017,** *146*, 054301.

[43]   Dermer, A. R.; Green, M. L.; Mascaritolo, K. J.; Heaven, M. C., Photoelectron Velocity Map Imaging Spectroscopy of the Beryllium Sulfide Anion, BeS^-. *J. Phys. Chem. A* **2017,** *121*, 5645-5650.

[44]   Delsart, C.; Goldfarb, F.; Blondel, C., Molecular photodetachment microscopy. *Phys. Rev. Lett.* **2002,** *89*.

[45]   Blondel, C.; Delsart, C.; Dulieu, F., The Photodetachment microscope. *Phys. Rev. Lett.* **1996,** *77*, 3755.

[46]   Weichman, M. L.; Neumark, D. M., Slow Photoelectron Velocity-Map Imaging of Cryogenically Cooled Anions. In *Annual Review of Physical Chemistry, Vol 69*, Johnson, M. A.; Martinez, T. J., Eds. 2018; Vol. 69, pp 101-124.

[47]   Babin, M. C.; DeVine, J. A.; DeWitt, M.; Stanton, J. F.; Neumark, D. M., High-Resolution Photoelectron Spectroscopy of Cryogenically Cooled NO_3^-. *J Phys Chem Lett* **2020,** *11*, 395-400.

[48]   Abou Taka, A.; Babin, M. C.; Sheng, X. H.; DeVine, J. A.; Neumark, D. M.; Hratchian, H. P., Unveiling the coexistence of cis- and trans-isomers in the hydrolysis of ZrO_2: A coupled DFT and high-resolution photoelectron spectroscopy study. *J. Chem. Phys.* **2020,** *153*, 244308.

[49]   DeVine, J. A.; Taka, A. A.; Babin, M. C.; Weichman, M. L.; Hratchian, H. P.; Neumark, D. M., High-resolution photoelectron spectroscopy of $TiO_3H_2^-$: probing the TiO_2^- + H_2O dissociative adduct. *J. Chem. Phys.* **2018,** *148*, 222810.

[50]   Babin, M. C.; DeWitt, M.; Lau, J. A.; Weichman, M. L.; Kim, J. B.; Song, H.; Guo, H.; Neumark, D. M., Observation of resonances in the transition state region of the F + NH3 reaction using anion photoelectron spectroscopy. *Nature Chem.* **2023,** *15*, 194-199.

[51]   DeWitt, M.; Babin, M. C.; Neumark, D. M., High-Resolution Photoelectron Spectroscopy of Vibrationally Excited OH^-. *J. Phys. Chem. A* **2021,** *125*, 7260-7265.

[52]   Lau, J. A.; DeWitt, M.; Boyer, M. A.; Babin, M. C.; Solomis, T.; Grellman, M.; Asmis, K. R.; McCoy, A. B.; Neumark, D. M., High-resolution photoelectron spectroscopy of vibrationally excited vinoxide anions. *J. Phys. Chem. A* **submitted**.

[53]   Wiley, W. C.; McLaren, I. H., Time-of-flight mass spectrometer with improved resolution. *Rev. Sci. Instrum.* **1955,** *26*, 1150-1157.

[54]   DeWitt, M.; Babin, M. C.; Lau, J. A.; Solomis, T.; Neumark, D. M., High Resolution Photoelectron Spectroscopy of the Acetyl Anion. *J. Phys. Chem. A* **2022,** *43*, 7962-7970.

[55]   Dick, B., Inverting ion images without Abel inversion: maximum entropy reconstruction of velocity maps. *Phys. Chem. Chem. Phys.* **2014,** *16*, 570-580.

[56]   Dick, B., MELEXIR: maximum entropy Legendre expanded image reconstruction. A fast and efficient method for the analysis of velocity map imaging or photoelectron imaging data. *Phys. Chem. Chem. Phys.* **2019,** *21*, 19499-19512.

[57]   Blondel, C.; Chaibi, W.; Delsart, C.; Drag, C.; Goldfarb, F.; Kröger, S., The electron affinities of O, Si, and Srevisited with the photodetachment microscope. *The European Physical Journal D - Atomic, Molecular, Optical and Plasma Physics* **2005,** *33*, 335-342.

[58]   Cooper, J.; Zare, R. N., Angular distribution of photoelectrons. *J. Chem. Phys.* **1968,** *48*, 942-943.

[59]   Reid, K. L., Photoelectron angular distributions. *Annu. Rev. Phys. Chem.* **2003,** *54*, 397-424.

[60]   Chappuis, J., Étude spectroscopique sur l'ozone. *Annales scientifiques de l'École Normale Supérieure* **1882,** *11*, 137-186.

[61] Monks, P. S., Gas-phase radical chemistry in the troposphere. *Chem. Soc. Rev.* **2005,** *34*, 376-395.

[62] Jones, E. J.; Wulf, O. R., The Absorption Coefficient of Nitrogen Pentoxide in the Ultraviolet and the Visible Absorption Spectrum of NO3. *J. Chem. Phys.* **1937,** *5*, 873-877.

[63] Graham, R. A.; Johnston, H. S., The photochemistry of the nitrate radical and the kinetics of the nitrogen pentoxide-ozone system. *J. Phys. Chem.* **1978,** *82*, 254-268.

[64] Ishiwata, T.; Fujiwara, I.; Naruge, Y.; Obi, K.; Tanaka, I., Study of nitrate radical by laser-induced fluorescence. *J. Phys. Chem.* **1983,** *87*, 1349-1352.

[65] Nelson, H. H.; Pasternack, L.; McDonald, J. R., Laser-induced excitation and emission spectra of nitrate radical (NO$_3$). *J. Phys. Chem.* **1983,** *87*, 1286-1288.

[66] Fukushima, M., Laser induced fluorescence spectra of the B ^{2}E' – X ^{2}A$_2$' transition of jet cooled ^{14}NO$_3$ and ^{15}NO$_3$ I: v$_4$ progressions in the ground X ^{2}A$_2$' state. *J. Mol. Spectrosc.* **2022,** *387*, 111646.

[67] Takematsu, K.; Eddingsaas, N. C.; Robichaud, D. J.; Okumura, M., Spectroscopic studies of the Jahn-Teller effect in the Ã^{2}E'' state of the nitrate radical NO$_3$. *Chem. Phys. Lett.* **2013,** *555*, 57-63.

[68] Codd, T.; Chen, M.-W.; Roudjane, M.; Stanton, J. F.; Miller, T. A., Jet cooled cavity ringdown spectroscopy of the A˜2E''←X˜2A2' transition of the NO3 radical. *J. Chem. Phys.* **2015,** *142*, 184305.

[69] Weaver, A.; Arnold, D. W.; Bradforth, S. E.; Neumark, D. M., Examination Of the ^{2}A$_2$' and ^{2}E'' States Of NO$_3$ By Ultraviolet Photoelectron Spectroscopy Of NO$_3^-$. *J. Chem. Phys.* **1991,** *94*, 1740-1751.

[70] Haller, E.; Köppel, H.; Cederbaum, L. S.; Niessen, W. v.; Bieri, G., Multimode Jahn–Teller and pseudo-Jahn–Teller effects in BF+3. *J. Chem. Phys.* **1983,** *78*, 1359-1370.

[71] Mayer, M.; Cederbaum, L. S.; Köppel, H., Ground state dynamics of NO3: Multimode vibronic borrowing including thermal effects. *J. Chem. Phys.* **1994,** *100*, 899-911.

[72] Stanton, J. F., On the vibronic level structure in the NO3 radical. I. The ground electronic state. *J. Chem. Phys.* **2007,** *126*, 134309.

[73] Ishiwata, T.; Tanaka, I.; Kawaguchi, K.; Hirota, E., Infrared diode laser spectroscopy of the NO$_3$ v$_3$ band. *J. Chem. Phys.* **1985,** *82*, 2196-2205.

[74] Simmons, C. S.; Ichino, T.; Stanton, J. F., The v$_3$ Fundamental in NO$_3$ Has Been Seen Near 1060 cm^{-1}, Albeit Some Time Ago. *J. Phys. Chem. Lett.* **2012,** *3*, 1946-1950.

[75] Stanton, J. F., Simulation of the dispersed fluorescence spectrum of the NO3 (B)over-tilde - (X)over-tilde origin vibronic band. *J. Mol. Spectrosc.* **2022,** *389*, 111690.

[76] Hirota, E., Assignment of the photoelectron spectrum of the nitrate anion NO$_3^-$ and vibronic interactions in the nitrate free radical. *J. Mol. Spectrosc.* **2018,** *343*, 81-84.

[77] Reed, K. J.; Zimmerman, A. H.; Anderson, H. C.; Brauman, J. I., Cross sections for photodetachment of electrons from negative ions near threshold. *J. Chem. Phys.* **1976,** *64*, 1368-1375.

[78] Signorell, R.; Merkt, F., General symmetry selection rules for the photoionization of polyatomic molecules. *Mol. Phys.* **1997,** *92*, 793-804.

[79] Ervin, K. M.; Lineberger, W. C., Photoelectron Spectra Of C$_2^-$ and C$_2$H$^-$. *J. Phys. Chem.* **1991,** *95*, 1167-1177.

[80] Asmis, K. R.; Taylor, T. R.; Neumark, D. M., Anion photoelectron spectroscopy of B$_2$N. *J. Chem. Phys.* **1999,** *111*, 8838-8851.

[81] Diebold, U., Perspective: A controversial benchmark system for water-oxide interfaces: H$_2$O/TiO$_2$(110). *J. Chem. Phys.* **2017,** *147*, 040901.

[82] Fasulo, F.; Piccini, G.; Muñoz-García, A. B.; Pavone, M.; Parrinello, M., Dynamics of Water Dissociative Adsorption on TiO$_2$ Anatase (101) at Monolayer Coverage and Below. *J. Phys. Chem. C* **2022,** *126*, 15752-15758.

[83] Fujishima, A.; Honda, K., Electrochemical Photolysis of Water at a Semiconductor Electrode. *Nature* **1972,** *238*, 37.

[84]   Sayama, K.; Arakawa, H., Photocatalytic decomposition of water and photocatalytic reduction of carbon dioxide over zirconia catalyst. *J. Phys. Chem.* **1993,** *97*, 531-533.

[85]   Linsebigler, A. L.; Lu, G.; Yates, J. T., Jr., Photocatalysis on TiO_2 Surfaces: Principles, Mechanisms, and Selected Results. *Chem. Rev.* **1995,** *95*, 735-758.

[86]   Wang, T.-H.; Fang, Z.; Gist, N. W.; Li, S.; Dixon, D. A.; Gole, J. L., Computational Study of the Hydrolysis Reactions of the Ground and First Excited Triplet States of Small TiO_2 Nanoclusters. *J. Phys. Chem. C* **2011,** *115*, 9344-9360.

[87]   Fang, Z.; Outlaw, M. D.; Smith, K. K.; Gist, N. W.; Li, S.; Dixon, D. A.; Gole, J. L., Computational Study of the Hydrolysis Reactions of Small MO_2 (M = Zr and Hf) Nanoclusters with Water. *J. Phys. Chem. C* **2012,** *116*, 8475-8492.

[88]   Fang, Z.; Dixon, D. A., Computational Study of H_2 and O_2 Production from Water Splitting by Small $(MO_2)_n$ Clusters (M = Ti, Zr, Hf). *J. Phys. Chem. A* **2013,** *117*, 3539-3555.

[89]   Cuko, A.; Macià Escatllar, A.; Calatayud, M.; Bromley, S. T., Properties of hydrated TiO2 and SiO2 nanoclusters: dependence on size, temperature and water vapour pressure. *Nanoscale* **2018,** *10*, 21518-21532.

[90]   Li, R.-Z.; Xu, H.-G.; Cao, G.-J.; Xu, X.-L.; Zheng, W.-J., Interaction of TiO_2^- with water: Photoelectron spectroscopy and density functional calculations. *J. Chem. Phys.* **2013,** *139*, 184303.

[91]   Weichman, M. L.; Debnath, S.; Kelly, J. T.; Gewinner, S.; Schöllkopf, W.; Neumark, D. M.; Asmis, K. R., Dissociative Water Adsorption on Gas-Phase Titanium Dioxide Cluster Anions Probed with Infrared Photodissociation Spectroscopy. *Top Catal* **2017**.

[92]   Yin, S.; Bernstein, E. R., Experimental and theoretical studies of H_2O oxidation by neutral $Ti_2O_{4,5}$ clusters under visible light irradiation. *Phys. Chem. Chem. Phys.* **2014,** *16*, 13900-13908.

[93]   Shirai, K.; Fazio, G.; Sugimoto, T.; Selli, D.; Ferraro, L.; Watanabe, K.; Haruta, M.; Ohtani, B.; Kurata, H.; Di Valentin, C.; Matsumoto, Y., Water-Assisted Hole Trapping at the Highly Curved Surface of Nano-TiO2 Photocatalyst. *J. Am. Chem. Soc.* **2018,** *140*, 1415-1422.

[94]   Kim, J. B.; Weichman, M. L.; Neumark, D. M., High-resolution anion photoelectron spectra of TiO_2^-, ZrO_2^-, and HfO_2^- obtained by slow electron velocity- map imaging. *Phys. Chem. Chem. Phys.* **2013,** *15*, 20973-20981.

[95]   Wenthold, P. G.; Hrovat, D. A.; Borden, W. T.; Lineberger, W. C., Transition-State Spectroscopy Of Cyclooctatetraene. *Science* **1996,** *272*, 1456-1459.

[96]   Wang, T.; Yang, T. G.; Xiao, C. L.; Sun, Z. G.; Zhang, D. H.; Yang, X. M.; Weichman, M. L.; Neumark, D. M., Dynamical resonances in chemical reactions. *Chem. Soc. Rev.* **2018,** *47*, 6744-6763.

[97]   Burnett, S. M.; Stevens, A. E.; Feigerle, C. S.; Lineberger, W. C., Observation of X^1A_1 Vinylidene by Photoelectron-Spectroscopy of the $C_2H_2^-$ Ion. *Chem. Phys. Lett.* **1983,** *100*, 124-128.

[98]   Manolopoulos, D. E.; Stark, K.; Werner, H. J.; Arnold, D. W.; Bradforth, S. E.; Neumark, D. M., The Transition State Of the $F+H_2$ Reaction. *Science* **1993,** *262*, 1852-1855.

[99]   Kim, J. B.; Weichman, M. L.; Sjolander, T. F.; Neumark, D. M.; Klos, J.; Alexander, M. H.; Manolopoulos, D. E., Spectroscopic observation of resonances in the $F + H_2$ reaction. *Science* **2015,** *349*, 510-513.

[100]   Garand, E.; Zhou, J.; Manolopoulos, D. E.; Alexander, M. H.; Neumark, D. M., Nonadiabatic interactions in the $Cl+H_2$ reaction probed by ClH_2^- and ClD_2^- photoelectron imaging. *Science* **2008,** *319*, 72-75.

[101]   Westermann, T.; Kim, J. B.; Weichman, M. L.; Hock, C.; Yacovitch, T. I.; Palma, J.; Neumark, D. M.; Manthe, U., Resonances in the Entrance Channel of the Elementary Chemical Reaction of Fluorine and Methane. *Angew. Chem., Int. Ed.* **2014,** *53*, 1122-1126.

[102]   Stang, P. J., Unsaturated carbenes. *Chem. Rev.* **1978,** *78*, 383-405.

[103]   Carrington, T.; Hubbard, L. M.; Schaefer, H. F.; Miller, W. H., Vinylidene - Potential-Energy Surface and Unimolecular Reaction Dynamics. *J. Chem. Phys.* **1984,** *80*, 4347-4354.

[104] Lee, H.; Baraban, J. H.; Field, R. W.; Stanton, J. F., High-Accuracy Estimates for the Vinylidene-Acetylene Isomerization Energy and the Ground State Rotational Constants of :C≡CH$_2$. *J. Phys. Chem. A* **2013,** *117*, 11679-11683.

[105] Han, H.; Li, A.; Guo, H., Toward spectroscopically accurate global ab initio potential energy surface for the acetylene-vinylidene isomerization. *J. Chem. Phys.* **2014,** *141*, 244312.

[106] Schaefer, H. F., III, The 1,2 hydrogen shift: a common vehicle for the disappearance of evanescent molecular species. *Accts. Chem. Res.* **1979,** *12*, 288-296.

[107] Levin, J.; Feldman, H.; Baer, A.; Ben-Hamu, D.; Heber, O.; Zajfman, D.; Vager, Z., Study of unimolecular reactions by Coulomb explosion imaging: The nondecaying vinylidene. *Phys. Rev. Lett.* **1998,** *81*, 3347-3350.

[108] Jacobson, M. P.; Field, R. W., Acetylene at the threshold of isomerization. *J. Phys. Chem. A* **2000,** *104*, 3073-3086.

[109] Jochim, B.; Berry, B.; Severt, T.; Feizollah, P.; Zohrabi, M.; P, K. R.; Wells, E.; Carnes, K. D.; Ben-Itzhak, I., Dependence on the Initial Configuration of Strong Field-Driven Isomerization of C2H2 Cations and Anions. *J. Phys. Chem. Lett.* **2019,** *10*, 2320-2327.

[110] Hayes, R. L.; Fattal, E.; Govind, N.; Carter, E. A., Long live vinylidene! A new view of the H$_2$C=C: -> HCCH rearrangement from ab initio molecular dynamics. *J. Am. Chem. Soc.* **2001,** *123*, 641-657.

[111] Schork, R.; Koppel, H., Barrier recrossing in the vinylidene-acetylene isomerization reaction: A five-dimensional ab initio quantum dynamical investigation. *J. Chem. Phys.* **2001,** *115*, 7907-7923.

[112] Zou, S. L.; Bowman, J. M.; Brown, A., Full-dimensionality quantum calculations of acetylene-vinylidene isomerization. *J. Chem. Phys.* **2003,** *118*, 10012-10023.

[113] Guo, L.; Han, H.; Ma, J.; Guo, H., Quantum Dynamics of Vinylidene Photodetachment on an Accurate Global Acetylene-Vinylidene Potential Energy Surface. *J. Phys. Chem. A* **2015,** *119*, 8488-8496.

[114] Ren, Y.; Bian, W., Mode-Specific Tunneling Splittings for a Sequential Double-Hydrogen Transfer Case: An Accurate Quantum Mechanical Scheme. *J. Phys. Chem. Lett.* **2015,** *6*, 1824-1829.

[115] Herman, M.; Perry, D. S., Molecular spectroscopy and dynamics: a polyad-based perspective. *Phys. Chem. Chem. Phys.* **2013,** *15*, 9970-9993.

[116] Hougen, J. T.; Merer, A. J., Extended permutation-inversion groups for simultaneous treatment of the rovibronic states of trans-acetylene, cis-acetylene, and vinylidene. *J. Mol. Spectrosc.* **2011,** *267*, 200-221.

[117] DeVine, J. A.; Weichman, M. L.; Zhou, X. Y.; Ma, J. Y.; Jiang, B.; Guo, H.; Neumark, D. M., Non-Adiabatic Effects on Excited States of Vinylidene Observed with Slow Photoelectron Velocity-Map Imaging. *J. Am. Chem. Soc.* **2016,** *138*, 16417-16425.

[118] DeVine, J. A.; Weichman, M. L.; Xie, C. J.; Babin, M. C.; Johnson, M. A.; Ma, J. Y.; Guo, H.; Neumark, D. M., Autodetachment from Vibrationally Excited Vinylidene Anions. *J Phys Chem Lett* **2018,** *9*, 1058-1063.

[119] Weichman, M. L.; DeVine, J. A.; Babin, M. C.; Li, J.; Guo, L. F.; Ma, J. Y.; Guo, H.; Neumark, D. M., Feshbach resonances in the exit channel of the F + CH$_3$OH -> HF + CH$_3$O reaction observed using transition-state spectroscopy. *Nature Chem.* **2017,** *9*, 950-955.

[120] Bradforth, S. E.; Arnold, D. W.; Metz, R. B.; Weaver, A.; Neumark, D. M., Spectroscopy of the Transition-State - Hydrogen Abstraction Reactions of Fluorine. *J. Phys. Chem.* **1991,** *95*, 8066-8078.

[121] Manocha, A. S.; Setser, D. W.; Wickramaaratchi, M. A., Vibrational-Energy Disposal in Reactions of Fluorine-Atoms with Hydrides of Group-Iii, Group-Iv and Group-V. *Chem. Phys.* **1983,** *76*, 129-146.

[122] Donaldson, D. J.; Parsons, J.; Sloan, J. J.; Stolow, A., Vibrational-Energy Partitioning in the Reaction of F-Atoms with NH$_3$ and ND$_3$. *Chem. Phys.* **1984,** *85*, 47-62.

[123] Wategaonkar, S.; Setser, D. W., Vibrational-Energy Disposal in the Reactions of F Atoms with NH$_3$, ND$_3$, N$_2$H$_4$, and CH$_3$ND$_2$. *J. Chem. Phys.* **1987,** *86*, 4477-4487.

[124]   Xiao, C. F.; Shen, G. L.; Wang, X. Y.; Fan, H. J.; Yang, X. M., Crossed Beams Study on the Dynamics of the F-Atom Reaction with Ammonia. *J. Phys. Chem. A* **2010,** *114*, 4520-4523.

[125]   EspinosaGarcia, J.; Corchado, J. C., Analytical surface for the reaction with no saddle-point $NH_3+F->NH_2+FH$. Application of variational transition state theory. *J. Phys. Chem. A* **1997,** *101*, 7336-7344.

[126]   Tian, L.; Zhu, Y.; Song, H.; Yang, M., Theoretical study of the $F(^2P) + NH_3 \rightarrow HF + NH_2$ reaction on an accurate potential energy surface: dynamics and kinetics. *Phys. Chem. Chem. Phys.* **2019,** *21*, 11385-11394.

[127]   Espinosa-Garcia, J.; Monge-Palacios, M., Theoretical Study of the $F+NH_3$ and $F+ND_3$ Reactions: Mechanism and Comparison with Experiment. *J. Phys. Chem. A* **2011,** *115*, 13759-13763.

[128]   Kasdan, A.; Herbst, E.; Lineberger, W. C., Laser photoelectron spectrometry of CH^-. *Chem. Phys. Lett.* **1975,** *31*, 78-82.

[129]   Engelking, P. C.; Lineberger, W. C., Laser photoelectron spectrometry of NH^-: Electron affinity and intercombination energy difference in NH. *J. Chem. Phys.* **1976,** *65*, 4323-4324.

[130]   Goldfarb, F.; Drag, C.; Chaibi, W.; Kröger, S.; Blondel, C.; Delsart, C., Photodetachment microscopy of the P, Q, and R branches of the $OH^-(v=0)$ to OH(v=0) detachment threshold. *J. Chem. Phys.* **2005,** *122*, 014308.

[131]   Owrutsky, J. C.; Rosenbaum, N. H.; Tack, L. M.; Saykally, R. J., The Vibration-Rotation Spectrum of the Hydroxide Anion (OH^-). *J. Chem. Phys.* **1985,** *83*, 5338-5339.

[132]   Jusko, P.; Asvany, O.; Wallerstein, A. C.; Brunken, S.; Schlemmer, S., Two-Photon Rotational Action Spectroscopy of Cold OH^- at 1 ppb Accuracy. *Phys. Rev. Lett.* **2014,** *112*.

[133]   Smith, J. R.; Kim, J. B.; Lineberger, W. C., High-resolution threshold photodetachment spectroscopy of OH-. *Phys. Rev. A* **1997,** *55*, 2036-2043.

[134]   Otto, R.; Von Zastrow, A.; Best, T.; Wester, R., Internal state thermometry of cold trapped molecular anions. *Phys. Chem. Chem. Phys.* **2013,** *15*, 612-618.

[135]   Rosenbaum, N. H.; Owrutsky, J. C.; Tack, L. M.; Saykally, R. J., Velocity Modulation Laser Spectroscopy of Negative-Ions - the Infrared-Spectrum of Hydroxide (OH^-). *J. Chem. Phys.* **1986,** *84*, 5308-5313.

[136]   Dousmanis, G. C.; Sanders, T. M.; Townes, C. H., Microwave Spectra of the Free Radicals OH and OD. *Phys. Rev.* **1955,** *100*, 1735-1755.

[137]   Beaudet, R. A.; Poynter, R. L., Microwave-Spectra of Molecules of Astrophysical Interest .12. Hydroxyl Radical. *J. Phys. Chem. Ref. Data* **1978,** *7*, 311-362.

[138]   Coxon, J. A., Optimum Molecular-Constants and Term Values for the $X^2\Pi(v\leq5)$ and $A^2\Sigma^+(v\leq3)$ States of OH. *Can. J. Phys.* **1980,** *58*, 933-949.

[139]   Melen, F.; Sauval, A. J.; Grevesse, N.; Farmer, C. B.; Servais, C.; Delbouille, L.; Roland, G., A new analysis of the OH radical spectrum from solar infrared observations. *J. Mol. Spectrosc.* **1995,** *174*, 490-509.

[140]   Robertson, W. H.; Johnson, M. A., Molecular aspects of halide ion hydration: The cluster approach. *Annu. Rev. Phys. Chem.* **2003,** *54*, 173-213.

[141]   Heine, N.; Asmis, K. R., Cryogenic ion trap vibrational spectroscopy of hydrogen-bonded clusters relevant to atmospheric chemistry. *Int. Rev. Phys. Chem.* **2015,** *34*, 1-34.

[142]   Kim, H. L.; Kulp, T. J.; McDonald, J. D., Infrared fluorescence study on the threshold of intramolecular vibrational state mixing. *J. Chem. Phys.* **1987,** *87*, 4376-4382.

[143]   Jackson, R. L.; Hiberty, P. C.; Brauman, J. I., Threshold resonances in the electron photodetachment spectrum of acetaldehyde enolate anion. Evidence for a low-lying, dipole-supported state. *J. Chem. Phys.* **1981,** *74*, 3705-3712.

[144]   Ellison, G. B.; Engelking, P. C.; Lineberger, W. C., Photoelectron spectroscopy of alkoxide and enolate negative ions. *J. Phys. Chem.* **1982,** *86*, 4873-4878.

[145]   Mead, R. D.; Lykke, K. R.; Lineberger, W. C.; Marks, J.; Brauman, J. I., Spectroscopy and Dynamics of the Dipole-Bound State of Acetaldehyde Enolate. *J. Chem. Phys.* **1984,** *81*, 4883-4892.

[146]   Alconcel, L. S.; Deyerl, H.-J.; Zengin, V.; Continetti, R. E., Structure and Energetics of Vinoxide and the X(^{2}A′′) and A(^{2}A′) Vinoxy Radicals. *J. Phys. Chem. A* **1999,** *103*, 9190-9194.

[147]   Yacovitch, T. I.; Garand, E.; Neumark, D. M., Slow photoelectron velocity-map imaging spectroscopy of the vinoxide anion. *J. Chem. Phys.* **2009,** *130*, 244309.

[148]   Endo, Y.; Saito, S.; Hirota, E., The microwave spectrum of the vinoxy radical. *J. Chem. Phys.* **1985,** *83*, 2026-2034.

[149]   Jacox, M. E., The reaction of F atoms with acetaldehyde and ethylene oxide. Vibrational spectra of the CH_3CO and CH_2CHO free radicals trapped in solid argon. *Chem. Phys.* **1982,** *69*, 407-422.

[150]   Utkin, Y. G.; Han, J. X.; Sun, F. G.; Chen, H. B.; Scott, G.; Curl, R. F., High-resolution jet-cooled and room temperature infrared spectra of the v_3 CH stretch of vinoxy radical. *J. Chem. Phys.* **2003,** *118*, 10470-10476.

[151]   Inoue, G.; Akimoto, H., Laser-Induced Fluorescence of the C_2H_3O Radical. *J. Chem. Phys.* **1981,** *74*, 425-433.

[152]   Dimauro, L. F.; Heaven, M.; Miller, T. A., Laser-Induced Fluorescence Study of the B2a′′-]X2a′′ Transition of the Vinoxy Radical in a Supersonic Free Jet Expansion. *J. Chem. Phys.* **1984,** *81*, 2339-2346.

[153]   Yamaguchi, M.; Momose, T.; Shida, T., Vibrational Analysis and Calculation of Franck-Condon Factors for the Vinoxy Radical *X*(^{2}*A′′*) and *B*(^{2}*A′′*) States. *J. Chem. Phys.* **1990,** *93*, 4211-4222.

[154]   Wan, R.; Chen, X.; Wu, F.; Weiner, B. R., Observation of new vibronic transitions in the B̃ ^{2}*A′′* – X̃ ^{2}*A′′* manifold of the CH_2CHO radical. *Chem. Phys. Lett.* **1996,** *260*, 539-544.

[155]   Brock, L. R.; Rohlfing, E. A., Spectroscopic Studies of the (B)over-Tilde(2)a′′-(X)over-Tilde(2)a′′ System of the Jet-Cooled Vinoxy Radical. *J. Chem. Phys.* **1997,** *106*, 10048-10065.

[156]   Osborn, D. L.; Choi, H.; Mordaunt, D. H.; Bise, R. T.; Neumark, D. M.; Rohlfing, C. M., Fast beam photodissociation spectroscopy and dynamics of the vinoxy radical. *J. Chem. Phys.* **1997,** *106*, 3049-3066.

[157]   Nielsen, H. H., The Vibration-Rotation Energies of Molecules. *Rev. Mod. Phys.* **1951,** *23*, 90-136.

[158]   Barone, V., Anharmonic vibrational properties by a fully automated second-order perturbative approach. *J. Chem. Phys.* **2005,** *122*, 014108.

[159]   Franke, P. R.; Stanton, J. F.; Douberly, G. E., How to VPT2: Accurate and Intuitive Simulations of CH Stretching Infrared Spectra Using VPT2+K with Large Effective Hamiltonian Resonance Treatments. *J. Phys. Chem. A* **2021,** *125*, 1301-1324.

[160]   Boyer, M. A.; McCoy, A. B., A flexible approach to vibrational perturbation theory using sparse matrix methods. *J. Chem. Phys.* **2022,** *156*, 054107.

[161]   Boyer, M. A.; McCoy, A. B., A wave function correction-based approach to the identification of resonances for vibrational perturbation theory. *J. Chem. Phys.* **2022,** *157*, 164113.

[162]   Lehmann, K. K.; Scoles, G.; Pate, B. H., Intramolecular Dynamics from Eigenstate-Resolved Infrared-Spectra. *Annu. Rev. Phys. Chem.* **1994,** *45*, 241-274.

[163]   Nesbitt, D. J.; Field, R. W., Vibrational Energy Flow in Highly Excited Molecules: Role of Intramolecular Vibrational Redistribution. *J. Phys. Chem.* **1996,** *100*, 12735–12756.

[164]   McDonald, J. D., Creation and Disposal of Vibration Energy in Polyatomic Molecules. *Annu. Rev. Phys. Chem.* **1979,** *30*, 29-50.
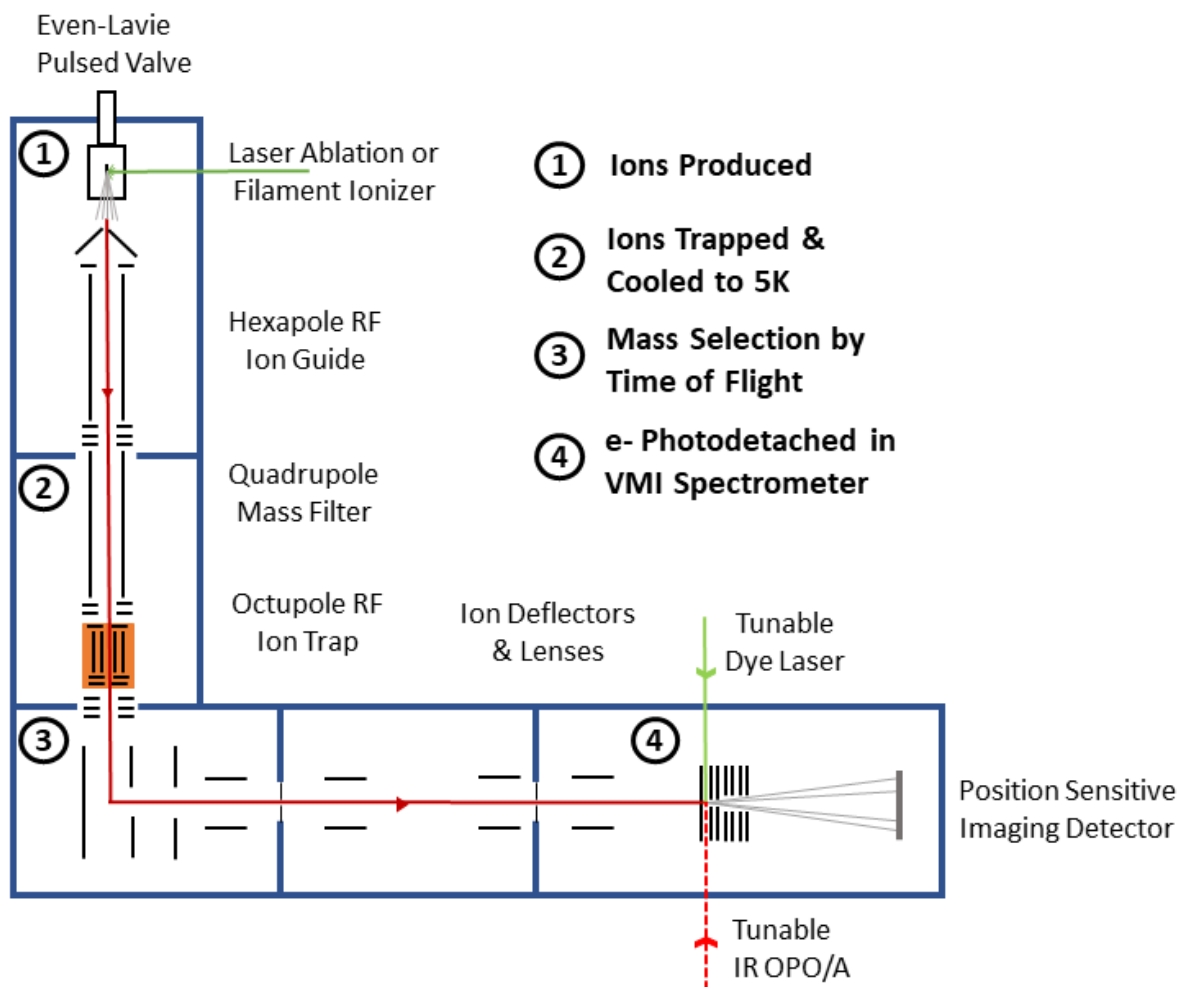
Figure 1. Schematic of current configuration of cryo-SEVI instrument, including the capability of infrared excitation of the anions prior to photodetachment.
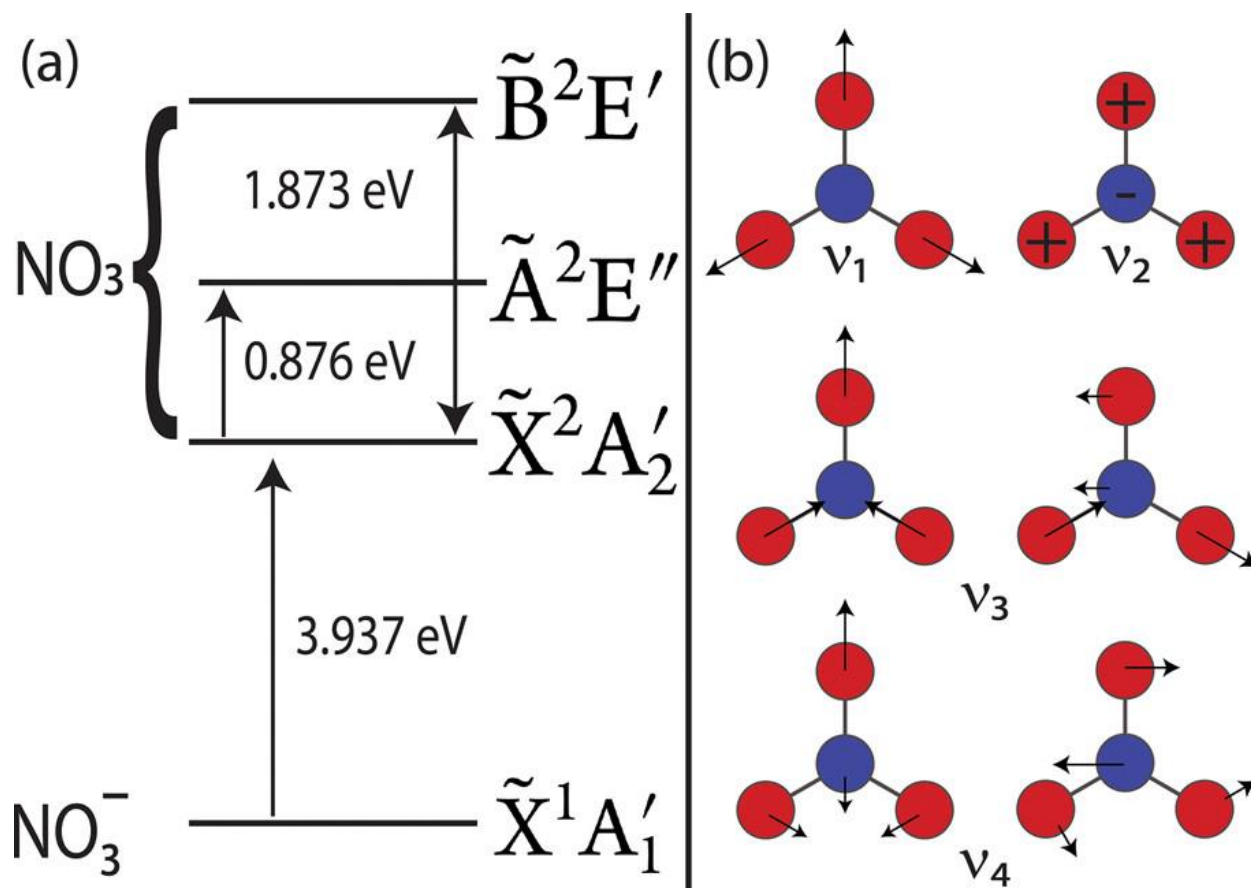
Figure 2. Schematic of the electronic energy levels of NO_3^- and NO_3 (left) and the vibrational modes of NO_3 (right).[47]
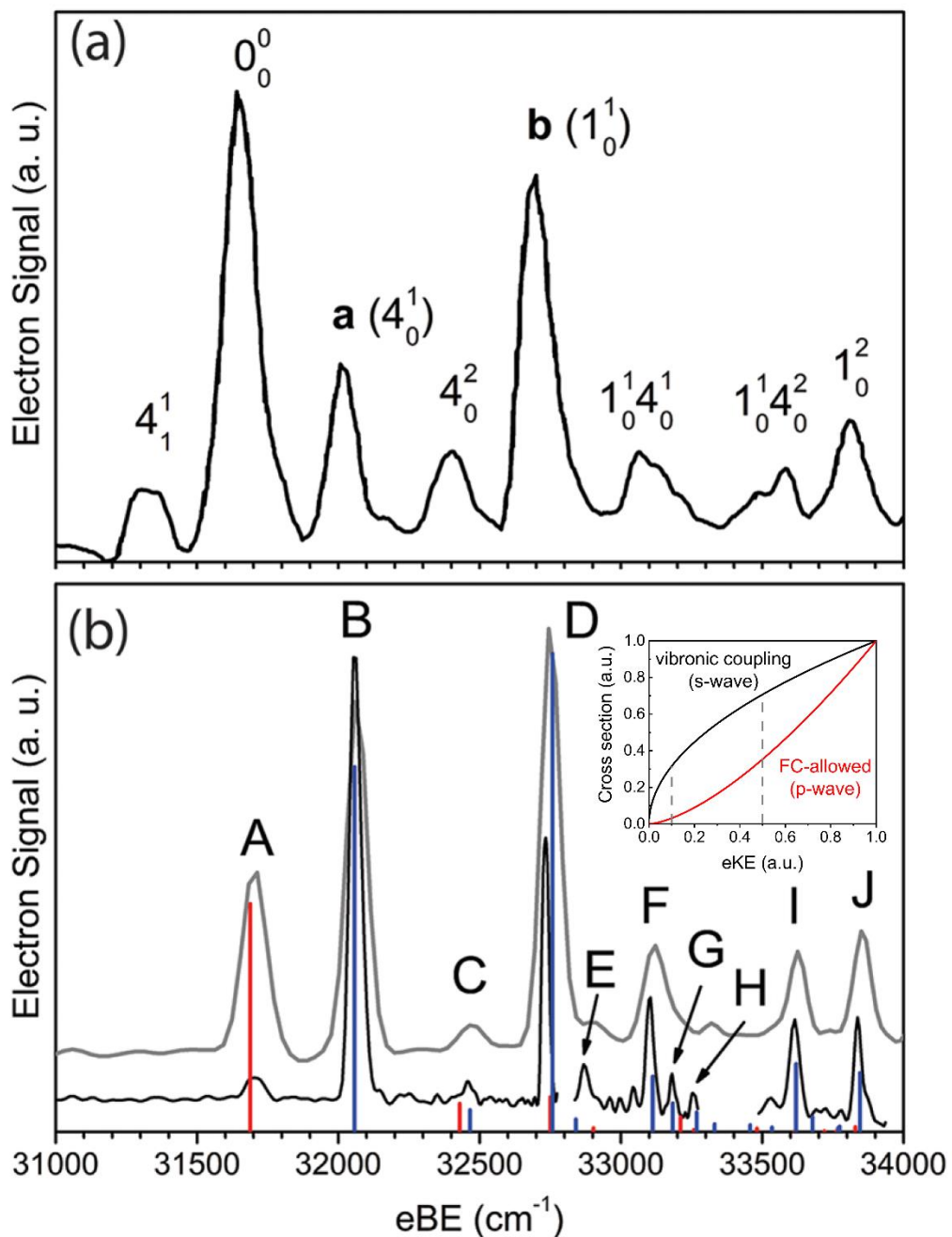
Figure 3. Anion photoelectron spectrum of NO_3^- (a) and cryo-SEVI spectrum (b).[47, 69] Stick spectrum in bottom panel is calculation showing transitions to Franck-Condon allowed (red) and forbidden (blue) levels of NO_3. Inset shows prediction of Wigner Threshold Law for s- and p-wave detachment.
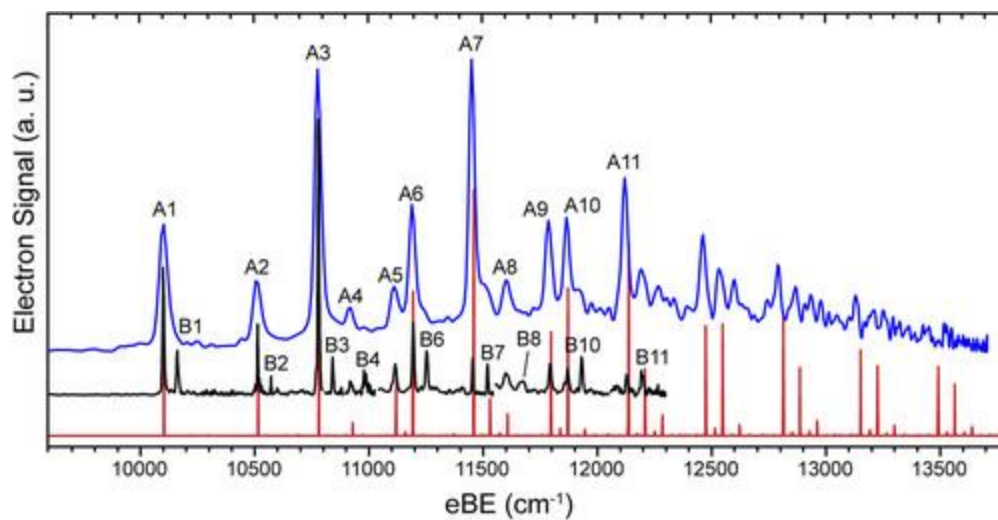
Figure 4. Cryo-SEVi spectrum of $TiO_2(OH)_2^-$.[49] Blue trace is overview spectrum and black trace is high-resolution composite spectrum The red sticks are from a Franck-Condon (FC) simulation. Peaks labeled "B" appear only in the high resolution spectrum. They are FC forbidden transitions and thus are absent in the FC simulation.
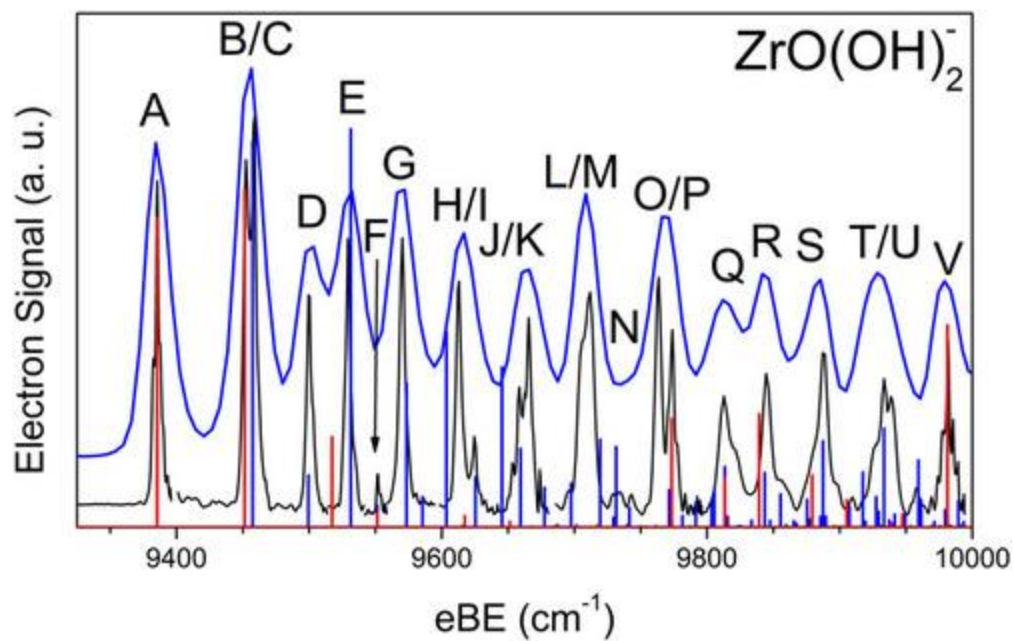
Figure 5. Cryo-SEVI spectra of $ZrO(OH)_2^-$.[48] Blue and black traces are overview and high-resolution composite spectra. Red and blue sticks are FC simulations starting from cis- and trans- anion isomers, respectively (see Figure 6),

Anion Structures

1-1a
0.00 eV

1-1b
0.07 eV

1-1c
2.14 eV

Neutral Structures

1-1a'
1.04 eV

1-1b'
1.11 eV

1-1c'
3.11 eV
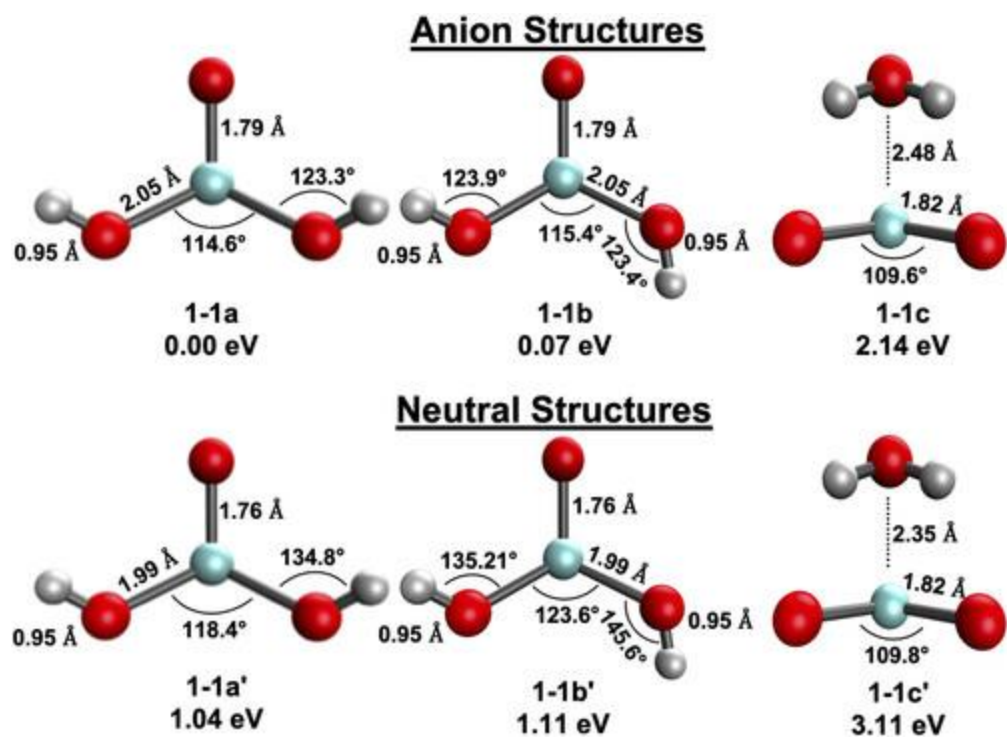
Figure 6.   Calculated structures and energetics for isomers of $ZrO_2(OH)_2^-$ (top) and $ZrO_2(OH)_2$ (bottom).[48]
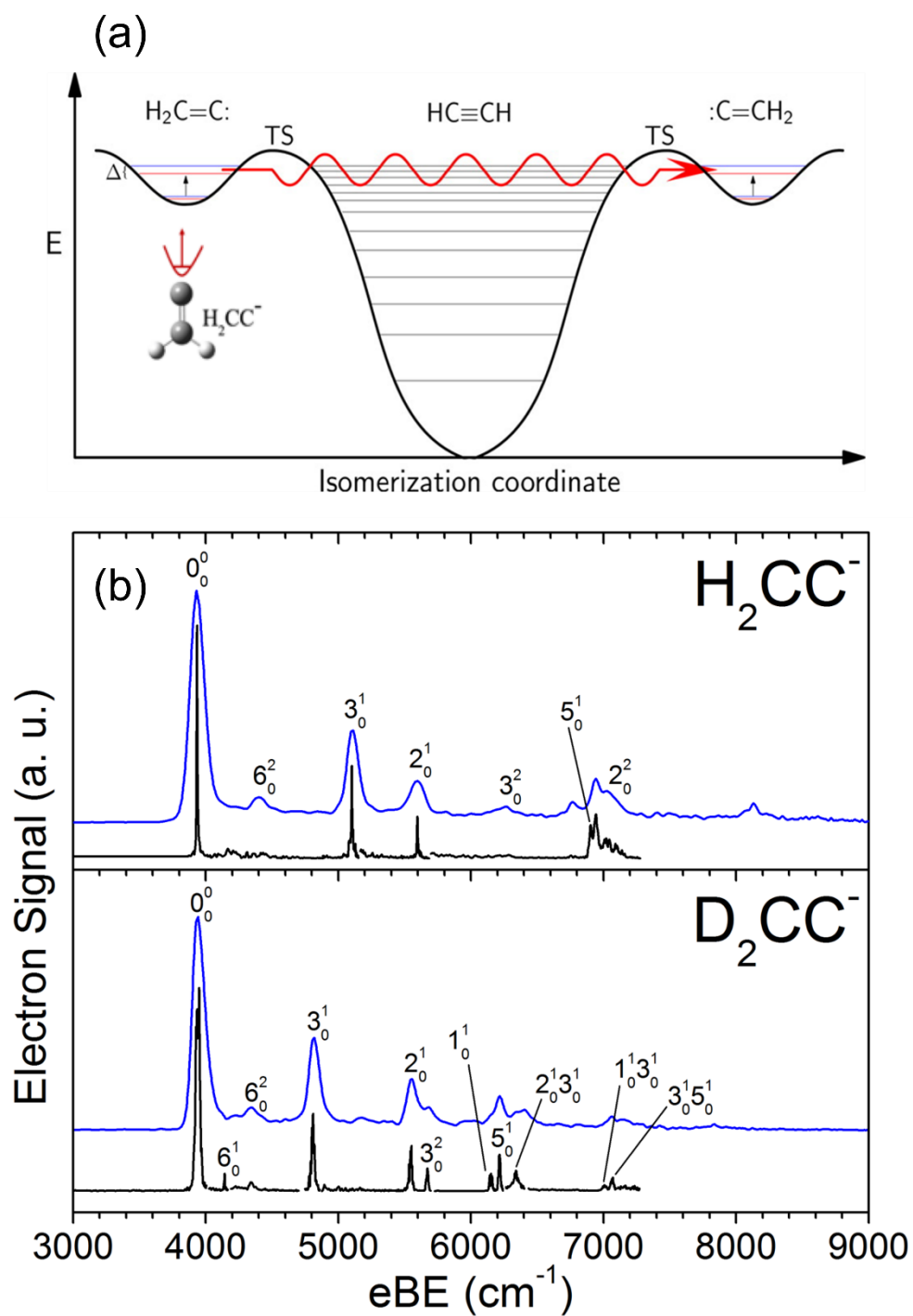
Figure 7. Schematic of $H_2CC \leftrightarrow HCCH$ isomerization coordinate (top).[114] Bottom panels show cryo-SEVI spectra of H_2CC^- and D_2CC^-.[13]
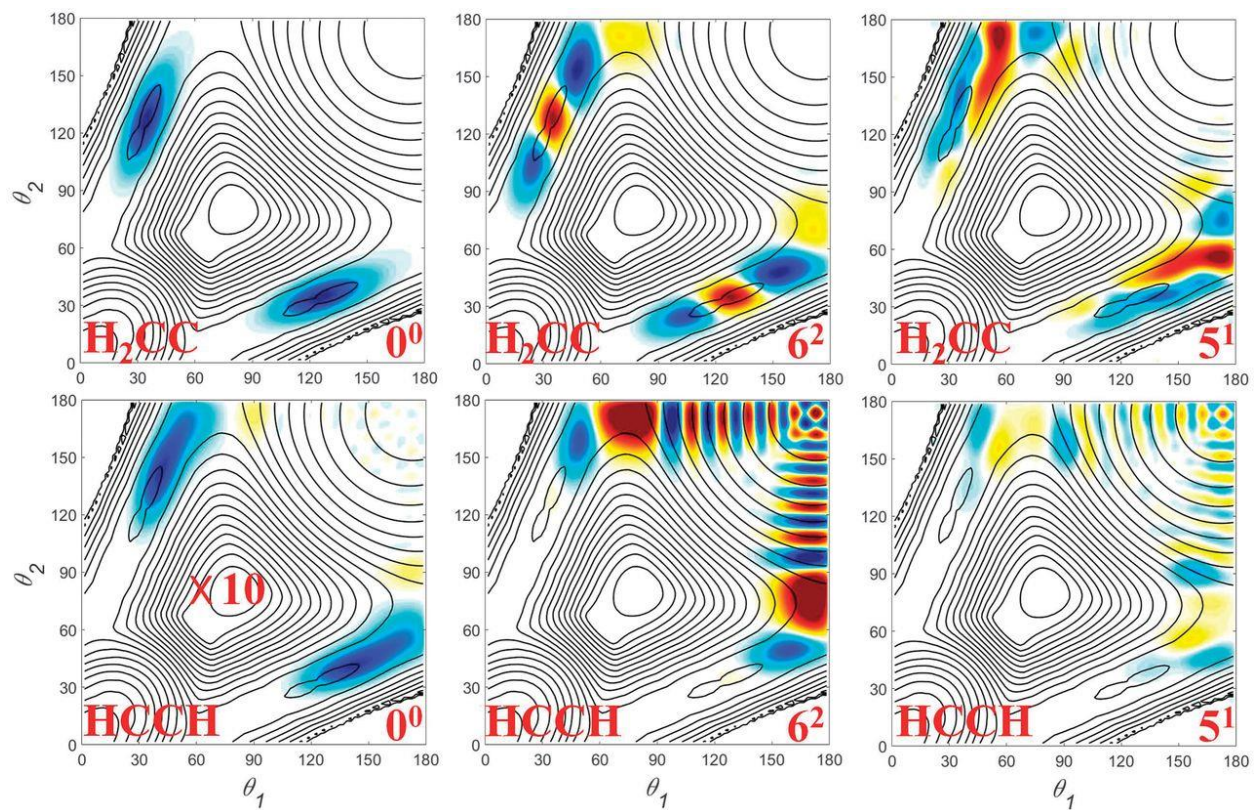
Figure 8. Calculated wavefunctions[13] for vibrational ground state (left), v_6=2 (center), and v_5=1 (right) vibrational states of H_2CC, projected onto H_2CC (top) and HCCH geometries (bottom).
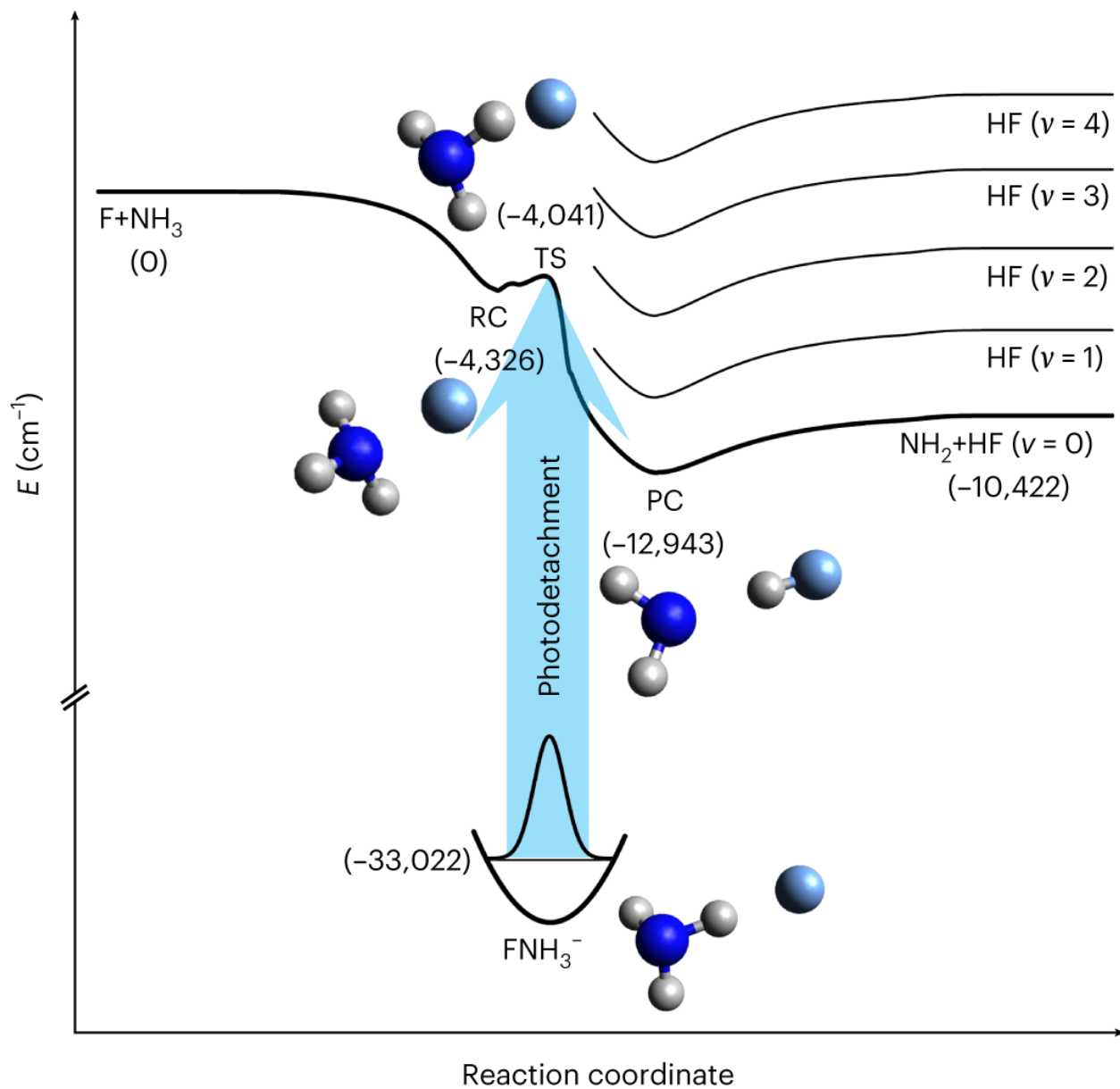
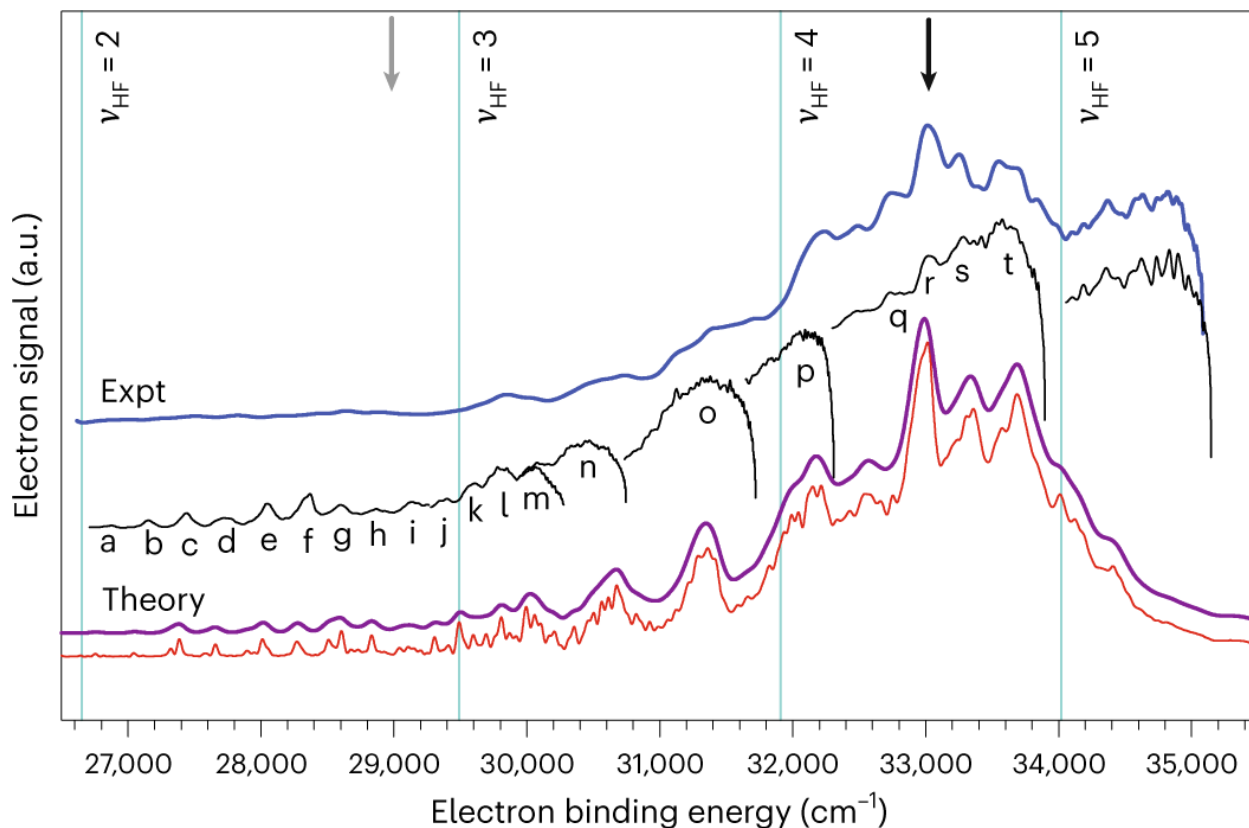Figure 9. Calculated reaction coordinate and energetics for F+NH₃ reaction (top) and FNH₃⁻ anion (bottom).[50]

Figure 10. Experimental (top two traces) and simulated (bottom two traces) cryo-SEVI spectra of FNH_3^-. Aqua vertical lines are energies of HF(v) + NH_2 product states. Grey and black arrows are energies of transition state and F + NH_3 reactant asymptote, respectively. Peak assignments are discussed in text.[50]
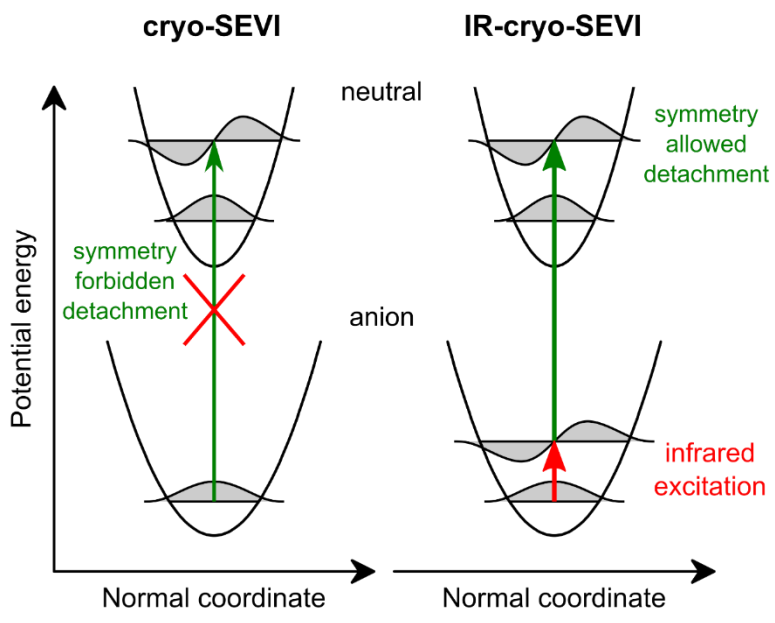
Figure 11. Principle of IR cryo-SEVI experiment. The v=1 level of a non-totally symmetric mode is generally inaccessible from the anion vibrational ground state (left). Vibrational pre-excitation of a non-totally symmetric mode activates new features in the cryo-SEVI spectrum (right).[52]
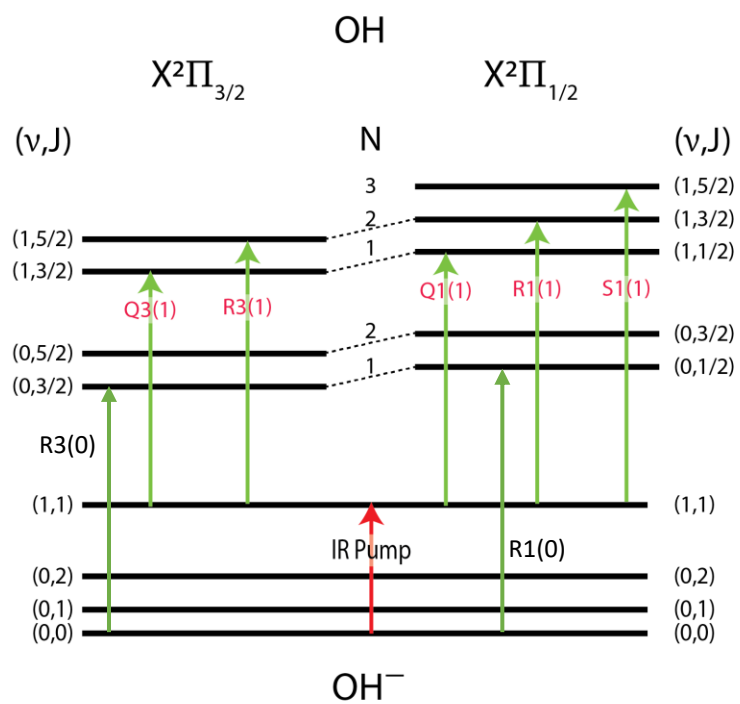
Figure 12. Vibration-rotation levels of OH‾ (bottom) and the two spin-orbit manifolds of OH (top). Selected photodetachment transitions (green) from the OH‾(0,0) and (1,1) states are shown. The IR laser vibrationally excites OH‾ via the R(0) transition.[51]

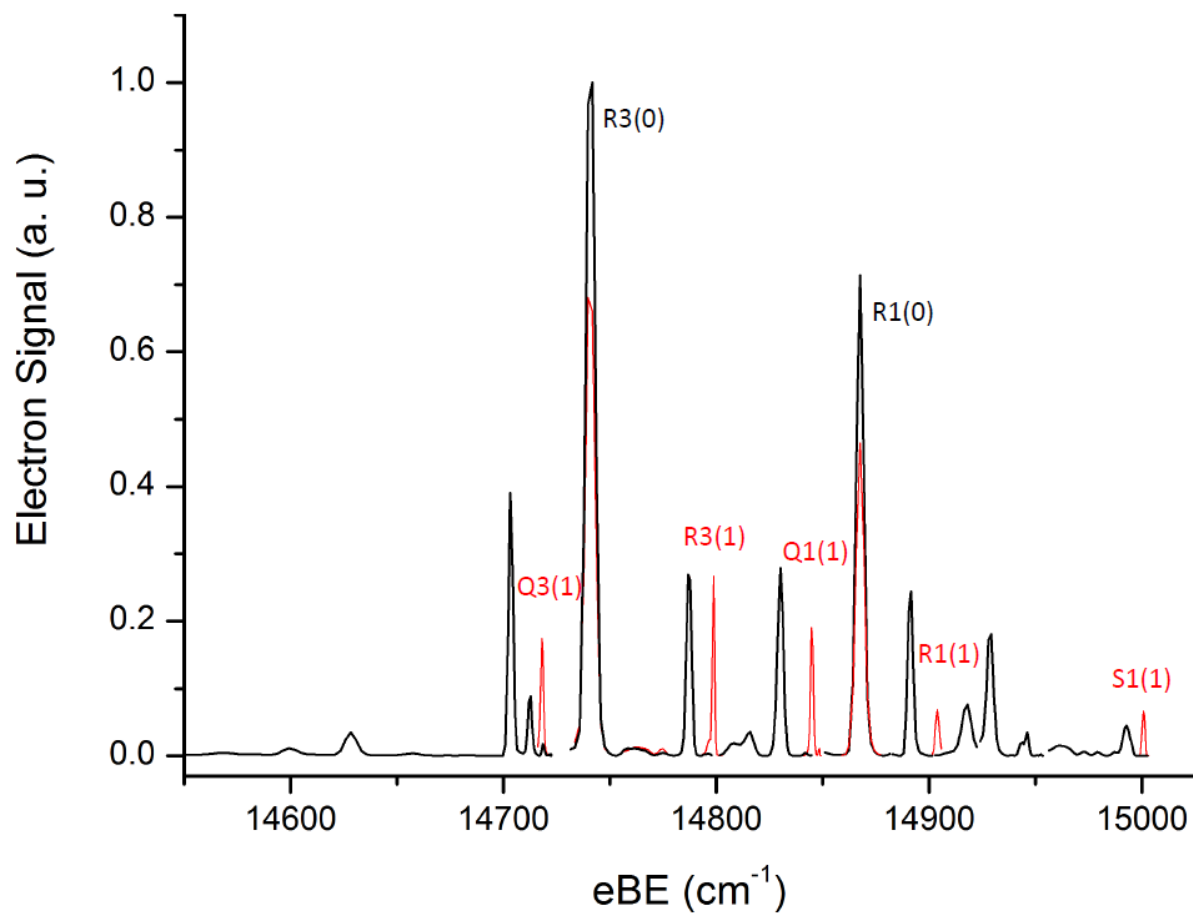Figure 13. Cryo-SEVI spectrum of cold (black) and vibrationally excited (red) OH⁻. Upon vibrational excitation, the R3(0) and R1(0) features are depleted and several new peaks appear.
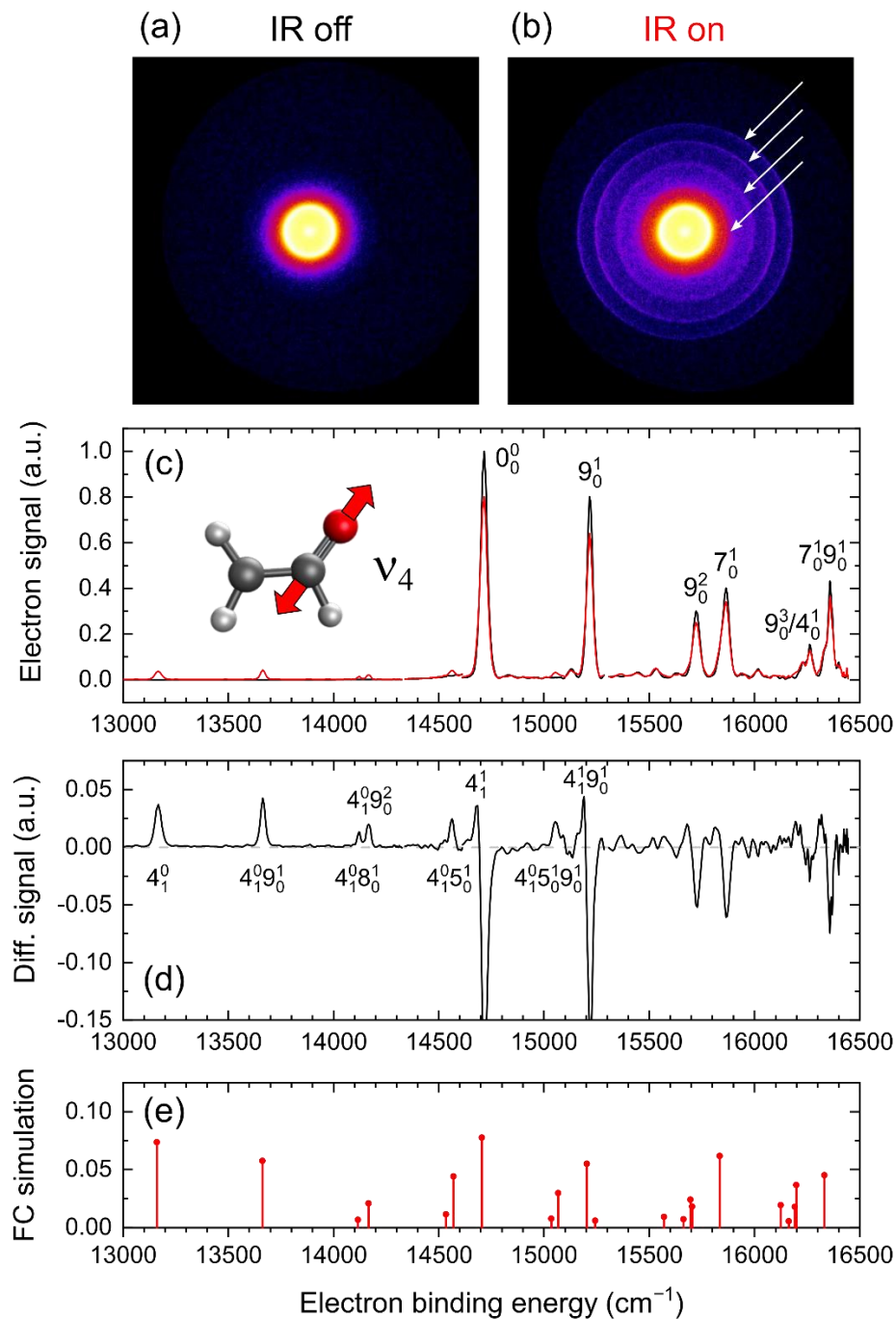
Figure 14. Excitation of the $\nu_4=1$ level of the vinoxide anion at 1570 cm^{-1}.[52] IR-off (a) and IR-on (b) photoelectron images show additional rings from IR excitation. Panel (c) compares IR-on (red) and IR-off (black) cryo-SEVI spectra, while (d) shows (IR-on)-(IR-off) difference spectrum. Positive and negative peaks originate from $\nu_4=1$ and $\nu_4=0$ levels of vinoxide, respectively. Panel (e) shows a simulated photoelectron spectrum from the anion $\nu_4=1$ level within harmonic and FC approximations.
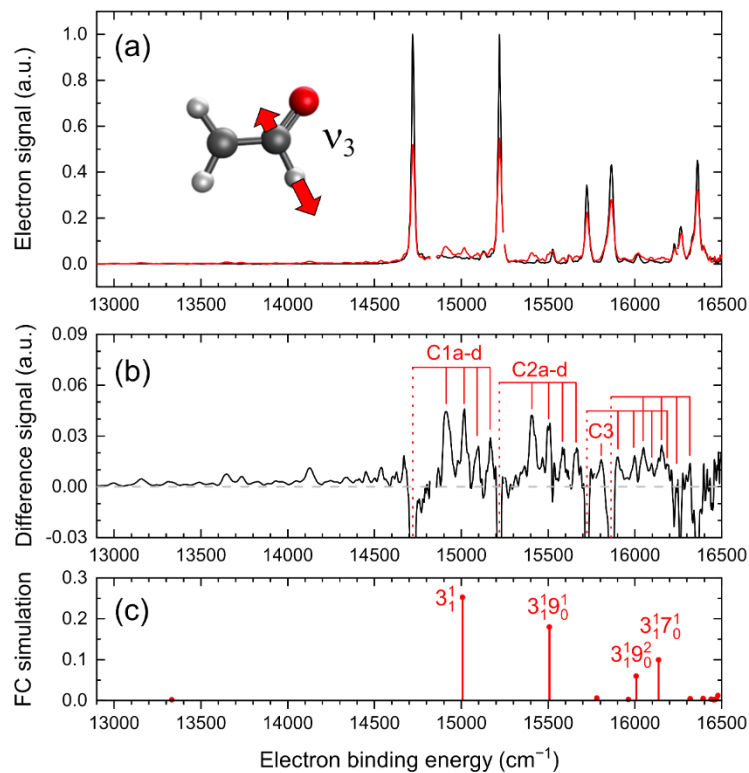
Figure 15. Effect of excitation of the ν_3=1 mode of vinoxide at 2546 cm^{-1}.[52] Panel (a) shows IR-on (red) and IR-off (black) cryo-SEVI spectra. Panel (b) shows the IR (on-off) difference spectrum. Panel (c) shows a FC simulation of the spectrum from the vinoxide ν_3=1 level within the harmonic approximation. Structure below and above the vibrational origin (0_0^0, see Figure 14) in panel (b) is from anharmonic coupling effects in the anion and neutral, respectively.

Zeroth-order neutral states

$|\phi'_{\nu_3}\rangle$

$|\phi'_{\nu_4+\nu_8}\rangle$

Photodetachment

Zeroth-order anion states

Coupled anion state

$|\chi''_i\rangle = c''_{\nu_3}|\phi''_{\nu_3}\rangle + c''_{\nu_4+\nu_8}|\phi''_{\nu_4+\nu_8}\rangle$

$|\phi''_{\nu_3}\rangle$

$|\phi''_{\nu_4+\nu_8}\rangle$

IR Excitation

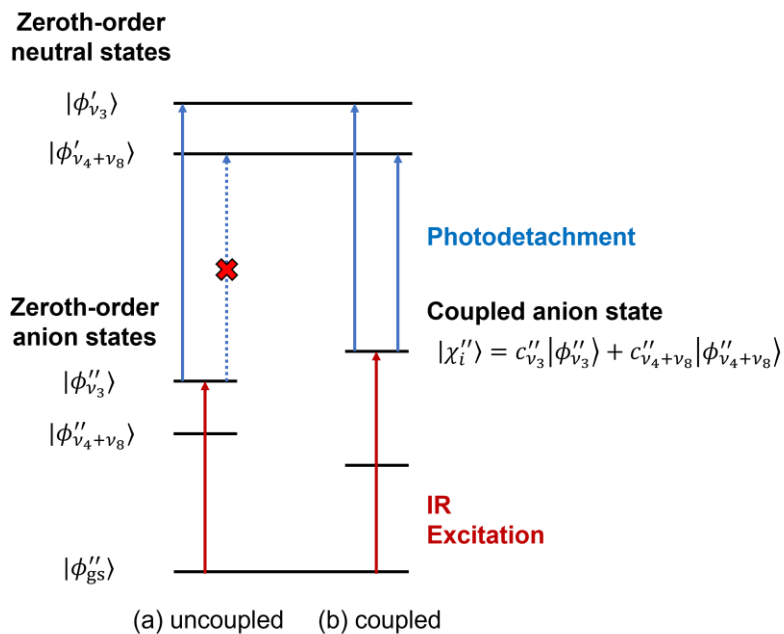$|\phi''_{gs}\rangle$

(a) uncoupled   (b) coupled

Figure 16. Mechanism for the appearance of new peaks in the cryo-SEVI spectrum owing to anharmonic coupling between anion vibrational levels. Photodetachment from the zeroth-order ν_3=1 anion state (left) only accesses the neutral ν_3=1 level (see FC simulation in panel (c) of Figure 15) while photodetachment if coupled anion state (right) accesses multiple neutral vibrational states.